Journal of Non-Newtonian Fluid Mechanics xxx (2012) xxx–xxx

Contents lists available at SciVerse ScienceDirect

Journal of Non-Newtonian Fluid Mechanics

journal homepage: http://www.elsevier.com/locate/jnnfm

Viscoplastic lubrication theory with application to bearings and the washboard instability of a planing plate

I.J. Hewitt [a,*], N.J. Balmforth [a,b]

[a] Department of Mathematics, University of British Columbia, Vancouver, BC, Canada V6T 1Z2
[b] Department of Earth & Ocean Science, University of British Columbia, Vancouver, BC, Canada V6T 1Z4

ARTICLE INFO

Article history:
Received 30 September 2011
Received in revised form 30 November 2011
Accepted 30 November 2011
Available online xxxx

Keywords:
Viscoplastic
Yield stress
Lubrication
Instability

ABSTRACT

We consider lubrication theory for a two-dimensional viscoplastic fluid confined between rigid moving boundaries. A general formulation is presented which allows the flow field and pressure to be calculated given an arbitrary rheological model; the Herschel–Bulkley law is used for illustration. The theory is first applied to a (full) viscoplastic journal bearing with arbitrary motions allowed for the inner cylinder (either prescribed, or arising from an imposed load and torque). Conditions are derived determining when motion is arrested by the yield stress. We next apply the theory to a slider bearing filled with Bingham fluid, computing the lift force on the bearing and the fluid flux through it. The results are then extended to model an inclined plate that is towed at constant horizontal speed over a shallow viscoplastic layer but is able to move vertically. Steady planing solutions are stable at low towing speeds, but give way to unstable vertical oscillations of the plate at higher speed; the yield stress has a relatively weak effect on this instability. The pattern imprinted on the fluid layer by the oscillations provides an analogue of the washboard phenomenon on gravel roads.

1. Introduction

A wide variety of lubrication problems involve the flow of non-Newtonian fluid between moving surfaces [1,2]. Our focus in the present article is lubrication by viscoplastic fluids, and, in particular, on the role of a yield stress. Although viscoplastic fluids are commonly used as lubricants (grease, for example, has previously been described as a Bingham fluid, e.g. [3,1]), the impact of a yield stress on the flow dynamics has not previously been fully explored. One explanation for this omission may be the complicated constitution of real lubricants, which defies an accurate description by idealized models such as the Bingham or Herschel–Bulkley laws. The operating conditions of many bearings also precludes yield stresses from playing an important dynamical role in practical situations [4]. On the other hand, yield stresses have recently been suggested as the key to stabilize lubricating multi-layer flows [5]. Moreover, in biological contexts, yield stresses may play an important role in peristaltic pumping [6,7] and animal locomotion problems, such as the swimming of a sperm [8], and the crawling of a snail [9,10].

The key difficulty in viscoplastic lubrication is that the yield stress can arrest flow over localized regions within the fluid. Importantly, the locations of these rigid plugs (or 'cores', as they are sometimes referred to) and how the flow pattern is organized around them may not be known at the outset. Instead, the yield surfaces are part of the solution of the problem in the fashion of a type of free-boundary problem. Complicating the problem further is that, in slender geometries, even if the fluid is yielded, the yield stress may still dominate the viscous stresses to create plug-like regions or "pseudo-plugs" [11,12].

In some situations, geometrical considerations can allow one to anticipate the pattern of plugs and pseudo-plugs and thereby more easily determine the flow field. Such considerations are exploited by existing solutions for viscoplastic slider and journal bearings [3,1,13,4], and underly the flow patterns for free-surface flows [14,12]. Nevertheless, in general settings, the flow pattern must be determined along with the solution, one implication of which is that in dynamical problems the plugs or pseudo-plugs may appear or disappear as the flow evolves. Such complications plague the swimming problems considered by Balmforth et al. [8] and Pegler [15], and constitute one of the difficulties that we address in the present article.

Our goal, then, is a general method for viscoplastic lubrication problems in which the flow pattern cannot be predicted ahead of time. In Section 2, we describe a general formulation of this method, following which, in Sections 3 and 4, we present two illustrative examples. The first, the viscoplastic journal bearing (Section 3), extends the work of Milne [3] and others [1,13] by allowing for general unsteady motion of the bearing surfaces. The applications of this analysis to real bearings are not so clear, in view of our restriction to full, non-cavitating, two-dimensional bearings

* Corresponding author. Tel.: +1 6048273296.
E-mail address: hewitt@math.ubc.ca (I.J. Hewitt).

0377-0257/$ - see front matter © 2011 Elsevier B.V. All rights reserved.
doi:10.1016/j.jnnfm.2011.11.008

filled with a model viscoplastic fluid (a Herschel–Bulkley fluid). Our purpose, however, is to use this classical type of bearing chiefly as a model problem to illustrate the difficulties and the features of the solutions. Accordingly, we focus on the dynamical behaviour of the bearing, rather than steady solutions of the Sommerfeld type as presented previously [3,1,13]. Along the way, we elucidate dynamics relevant to sedimentation problems. In particular, the thin-gap geometry of the bearing allows us to make considerable analytical headway into exploring how a cylinder sediments through a viscoplastic fluid towards a wall, with its progress arrested by the yield stress. The corresponding problem for a cylinder falling through an unbounded yield-stress fluid is rather more complicated owing to the convoluted structure of the yield surfaces and pseudo-plugs [17,18], and we are aware of no existing results for sedimentation towards a plane wall (unlike the Newtonian version which is a classic problem in viscous fluid mechanics [19]).

Our second example, in Section 4, is motivated by experiments on the phenomenon of washboard roads [20–22]. This phenomenon is usually thought of as a practical pattern-formation problem originating from the passage of a vehicle with a suspension over a sand or gravel surface. However, as alluded to by Mather [20] and demonstrated experimentally by Hewitt et al. [16] the surface need not be granular (many fluids can apparently be "washboarded") and the vehicle can simply be an inclined plate towed at constant speed. In the version of the problem explored here, the inclined plate is towed over a thin layer of a viscoplastic fluid; images from the corresponding experiment are shown in Fig. 1. Within the framework of lubrication theory, the dynamics can be discussed relatively concisely and the washboarding instability demonstrated theoretically. In fact, the idealized geometry we adopt makes this problem similar to two other standard lubrication problems: the slider bearing [1] and blade coating [23]. In Section 4, we therefore also revisit and extend some earlier work on sliders and blades moving over viscoplastic fluids.

The principal difference in the washboarding problem is that the inclined plate is free to move vertically according to the imposed gravitational load and the opposing fluid lift force, unlike the standard lubrication problems, where the plate position is held fixed. Despite this, we begin our study of the washboard instability by constructing the steady planing states in which the plate is dragged at fixed height over the layer, and which have a close relation to the slider bearing and blade coater. With that solution in hand, we then explore whether the plate is stable towards vertical oscillations (this unsteady problem has some similarities with the oscillations of an air slider bearing studied in [24]). We do indeed find that oscillations can grow unstably, generating periodic undulations of the plate that imprint a washboard pattern in the fluid layer left behind (*cf.* Fig. 1). The generality of both the experiments and theory suggests that this washboarding instability may well play a role in other problems, such as blade coating with pivoted or flexible blades [25]. It also turns out that the imprint carved by the plate features sharp steps that undoubtedly would be smoothed by gravity or surface tension. Thus, the passage of the washboarding plate leaves behind an adjusting fluid layer in which cliffs slump back to equilibrium in a novel variant of the free-surface flow problem [14,12,26].

We conclude our study in Section 5, and the Appendices contain a number of technical details that underscore many of the results described in the main text.

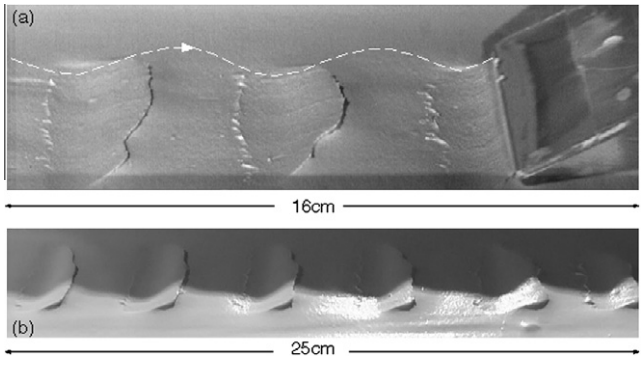

Fig. 1. An experiment in which an inclined plate is towed at constant speed over the surface of a layer of viscoplastic fluid [16]. The plate is pivoted so that it can move freely up and down under the action of gravity and the lift force from the fluid (when the plate and fluid are in contact). If the towing speed is sufficiently fast, the plate oscillates vertically due to an unstable interaction with the deforming fluid layer, leaving the surface between regularly spaced impacts and sculpting a washboard pattern in its wake. The top picture shows an image captured from high-speed video footage; the dashed line indicates the path taken by the far corner of the trailing edge of the plate. The lower picture shows a photograph taken of a longer section of the final washboard pattern; a shadow cast over the layer highlights the relief of the washboard (the peak-to-trough elevation differences are less than 2 mm). The towing speed was 37 cm/s, fluid depth was 7 mm, and the plate angle was 15°; the fluid is joint compound (a commercially available kaolin-based material), mixed with a little water, and possesses a yield stress of about 30 Pa.

2. Mathematical formulation

The lubrication problem centres on the two-dimensional flow of viscoplastic fluid within a narrow gap, as sketched generically in Fig. 2a, and for our specific examples in panels (b) and (c). For each of these problems. the gap is described by a Cartesian coordinate system which is orientated with x running approximately along the gap, and y directed across it. The surfaces bordering the gap are denoted $y = Y_1(x,t)$ and $y = Y_2(x,t)$, with the thickness, $h(x,t) = Y_2 - Y_1$. Along these surfaces, the velocities are $(U_1(x,t), V_1(x,t))$ and $(U_2(x,t), V_2(x,t))$.

2.1. Lubrication analysis

The gap has a characteristic thickness, $\mathcal{H}$, and length, $\mathcal{L}$; fluid flows through the gap with a characteristic speed of $\mathcal{U}$, and the cross-slot speeds are order $\mathcal{U}\mathcal{H}/\mathcal{L}$. For the lubrication analysis, we demand $\mathcal{H} \ll \mathcal{L}$, and assume that the reduced Reynolds number $(\mathcal{H}/\mathcal{L})\mathrm{Re} \ll 1$, where $\mathrm{Re} = \mathcal{U}\mathcal{H}/\nu$ and ν is a characteristic kinematic viscosity. These scales can be exploited to express all lengths and velocities in dimensionless form. We further add the timescale, $\mathcal{L}/\mathcal{U}$, and assume that shear stresses scale with $\mathcal{T} = \rho\nu\mathcal{U}/\mathcal{H}$, and pressures with $\mathcal{L}\mathcal{T}/\mathcal{H}$ (guaranteeing the lubrication pressures greatly exceed shear stresses); ρ is the fluid density. To leading order in the aspect ratio of the gap, $\mathcal{H}/\mathcal{L}$, the momentum and continuity equations for the fluid can be written in the dimensionless form

$$p_x = \tau_y, \quad p_y = 0, \quad u_x + v_y = 0, \tag{1}$$

where $p(x,t)$ is the fluid pressure, $\tau(x,y,t)$ is the shear stress, and the x and y subscripts denote partial derivatives. Gravity is ignored.

The boundary conditions are that

$$u(x,Y_1,t) = U_1, \quad v(x,Y_1,t) = V_1 \equiv Y_{1t} + U_1 Y_{1x}, \tag{2}$$

$$u(x,Y_2,t) = U_2, \quad v(x,Y_2,t) = V_2 \equiv Y_{2t} + U_2 Y_{2x}. \tag{3}$$

The momentum equations are integrated to furnish

$$\tau = \tau_1 + (y - Y_1)p_x = \tau_2 - (Y_2 - y)p_x, \tag{4}$$

where τ_1 and τ_2 are the surface shear stresses, which satisfy

$$p_x = \frac{1}{h}(\tau_2 - \tau_1). \tag{5}$$

For our viscoplastic fluids, when the shear rate, u_y, dominates the other strain rates, the constitutive law, to leading order, can be written in scalar form and in terms of a prescribed function:

Please cite this article in press as: I.J. Hewitt, N.J. Balmforth, Viscoplastic lubrication theory with application to bearings and the washboard instability of a planing plate, J. Non-Newtonian Fluid Mech. (2012), doi:10.1016/j.jnnfm.2011.11.008

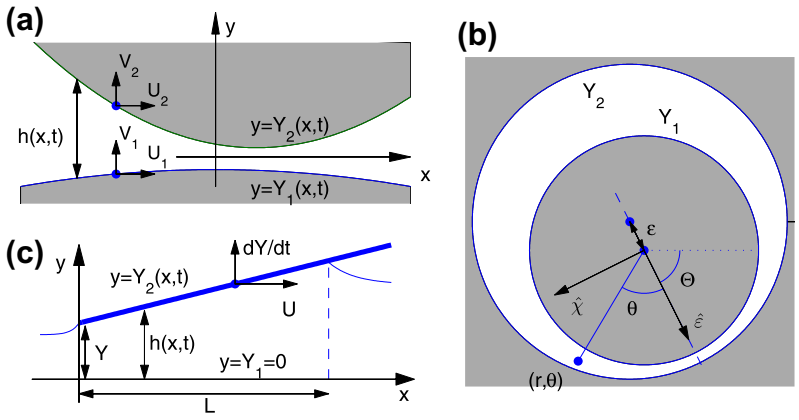

Fig. 2. Three sample geometries: (a) colliding smooth surfaces with an intervening viscoplastic fluid; (b) a viscoplastic journal bearing; and (c) a plate planing over a viscoplastic layer.

$\tau = T(u_y)$. Note that, for a yield-stress fluid, the rigid phase (with $u_y = 0$) corresponds to $T(u_y)$ being multi-valued over the range of stress beneath the yield value. More usefully, we define the (well-defined) inverse, $u_y = \Gamma(\tau)$. A sketch of $\Gamma(\tau)$ for the Herschel–Bulkley law is given in Fig. 3. This model, in our dimensionless notation, takes the form,

$$u_y = \Gamma(\tau) = (|\tau| - B)_+^{1/n}\ \mathrm{sgn}(\tau), \tag{6}$$

where $(\cdot)_+$ indicates $\max(\cdot,0)$, n is a power-law index and the Bingham number B is a dimensionless yield stress, with

$$B = \frac{\tau_Y}{\mathcal{T}} = \frac{\tau_Y \mathcal{H}}{\rho \nu \mathcal{U}}, \quad \rho\nu \equiv \frac{K\mathcal{U}^{n-1}}{\mathcal{H}^{n-1}}; \tag{7}$$

τ_Y is the dimensional yield stress and K is the consistency. In this one-dimensional form of the model, the fluid is yielded for $|\tau| \geqslant B$ and rigid otherwise; in the lubrication approximation of a two-dimensional fluid, however, the yield condition must be interpreted a little more carefully, as outlined by Balmforth and Craster [12] and mentioned later.

Exploiting the boundary conditions in (2) and (3), we may write

$$U \equiv U_2 - U_1 = \int_{Y_1}^{Y_2} u_y\ \mathrm{d}y \equiv \frac{1}{p_x}\int_{\tau_1}^{\tau_2} \Gamma(\tau)\ \mathrm{d}\tau, \tag{8}$$

in view of (4). If we define the new functions,

$$I_j(\tau) = \int \tau^j \Gamma(\tau)\ \mathrm{d}\tau, \tag{9}$$

then,

$$\frac{U}{h}(\tau_2 - \tau_1) = I_0(\tau_2) - I_0(\tau_1). \tag{10}$$

Also, the $y-$ integral of the continuity relation in (1) implies

$$\frac{\partial}{\partial x}\int_{Y_1}^{Y_2} u\ \mathrm{d}y + h_t = 0. \tag{11}$$

The x-integral thus implies

$$\begin{aligned} Q(t) &= \int_{Y_1}^{Y_2} u\ \mathrm{d}y + \int_0^x h_t(\hat{x},t)\ \mathrm{d}\hat{x} \\ &\equiv \frac{1}{2}\int_{Y_1}^{Y_2} (Y_2 + Y_1 - 2y)u_y\ \mathrm{d}y + q(x,t), \end{aligned} \tag{12}$$

where $Q(t)$ is a "constant" of integration that has the physical interpretation of a flux through $x = 0$, and

$$q(x,t) = \int_0^x h_t(\hat{x},t)\ \mathrm{d}\hat{x} + \frac{1}{2}h(U_1 + U_2). \tag{13}$$

Therefore

$$Q - q = \frac{hU(\tau_2 + \tau_1)}{2(\tau_2 - \tau_1)} - \frac{h^2[I_1(\tau_2) - I_1(\tau_1)]}{(\tau_2 - \tau_1)^2}. \tag{14}$$

Eqs. (10) and (14) constitute a pair of algebraic equations that must be solved at each position in x, given the gap thickness, h, surface velocities, (U_j, V_j), and the flux, $Q(t)$. In most situations, however, the flux is not prescribed, and instead one must impose pressure conditions at the two ends of the gap. In particular, there is a prescribed pressure difference across the gap of

$$P(t) = \int_D p_x\ \mathrm{d}x, \tag{15}$$

where D refers to the interval of x spanned by the fluid gap. With (5), we then arrive at the additional integral constraint,

$$P = \int_D (\tau_2 - \tau_1)\frac{\mathrm{d}x}{h}, \tag{16}$$

which determines Q. We present a convenient numerical algorithm to solve (10), (14) and (16) in Appendix A.

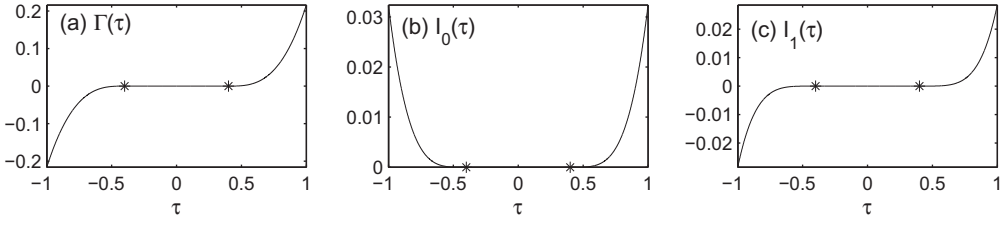

Fig. 3. The functions (a) $\Gamma(\tau)$, (b) $I_0(\tau)$ and (c) $I_1(\tau)$ for the Herschel–Bulkley model in lubrication approximation, with $\tau = T(u_y) = (B + |u_y|^n)\mathrm{sgn}(u_y)$ for $u_y \neq 0$, or $u_y = \Gamma(\tau) = (|\tau| - B)_+^{1/n}\ \mathrm{sgn}(\tau)$, where $B = 0.4$ is the Bingham number and $n = 1/3$ the power-law index. The yield points, $|\tau| = B$, are indicated by stars.

Please cite this article in press as: I.J. Hewitt, N.J. Balmforth, Viscoplastic lubrication theory with application to bearings and the washboard instability of a planing plate, J. Non-Newtonian Fluid Mech. (2012), doi:10.1016/j.jnnfm.2011.11.008

2.2. Yield surfaces and plugged regions

Once we solve this integro-algebraic system, we may reconstruct the flow field. Importantly, for a material with a yield stress, the fluid is predicted to yield when the magnitude of the shear stress attains the yield value B. The two conditions, $\tau = \pm B$, imply yield surfaces at the levels,

$$Y_\pm = Y_1 - \frac{\tau_1}{p_x} \pm \frac{B}{|p_x|}. \tag{17}$$

For $y > Y_+$ and $y < Y_-$, the fluid is fully yielded. Over the interval $Y_- < y < Y_+$, the fluid is dominated by the yield stress. As described by Balmforth and Craster [12], however, this region is not necessarily rigid, but can be held just above the yield stress, with the extensional stresses becoming of the same order as the shear stress. The region is then weakly yielded and more precisely referred to as a "pseudo-plug", with its borders signifying "fake" yield surfaces. The velocity profile across the pseudo-plugs is independent of y to leading order, but varies with x. Only if that velocity profile turns out to be independent of x is the region a true plug flow. This can be ascertained from the plug speed, u_b, which follows from the integrals, $\int_{Y_1}^{Y_-} u_y dy = -I_0(Y_1)/p_x = u_p - U_1$ or $\int_{Y_+}^{Y_2} u_y dy = I_0(Y_2)/p_x = U_2 - u_p$. That is,

$$u_p = U_1 - \frac{I_0(\tau_1)}{p_x} = U_2 - \frac{I_0(\tau_2)}{p_x}. \tag{18}$$

If the surface stresses both exceed the yield stress, $|\tau_j| > B$ for $j = 1$ and 2, but have opposite sign, then $Y_1 < Y_- < Y_+ < Y_2$ and u_p differs from U_1 and U_2, varying with x; *i.e.* the layer contains a pseudo-plug. On the other hand, if both surface stresses exceed the yield stress and have the same sign, $Y_\pm$ lie outside the gap and the layer is fully yielded. If $|\tau_1| < B$ and $|\tau_2| > B$, the plug is rigidly attached to the lower boundary, and moves with speed U_1 (in that case, $Y_- < Y_1 < Y_+ < Y_2$). Conversely if $|\tau_1| > B$ and $|\tau_2| < B$, a rigid plug is attached to the upper boundary and travels with speed U_2 (corresponding to $Y_1 < Y_- < Y_2 < Y_+$). The only other possibility is the uninteresting case $|\tau_j| < B j = 1$ and 2, for which the fluid layer must be unyielded and the surfaces unable to move relative to each other.

Based upon the surface shear stresses or the positions of the yield surfaces, we can therefore classify four different types of flow field:

- A: Central pseudo-plug; $|\tau_1|, |\tau_2| > B$ and $\mathrm{sgn}(\tau_1) = -\mathrm{sgn}(\tau_2)$.
- B: Lower plug; $|\tau_1| < B$.
- C: Fully yielded zone; $|\tau_1|, |\tau_2| > B$ and $\mathrm{sgn}(\tau_1) = \mathrm{sgn}(\tau_2)$.
- D: Upper plug; $|\tau_2| < B$.

As detailed in Appendix B, the governing Eqs. (10) and (14) for the Herschel–Bulkley model can be simplified in regions B and D, with analytical forms found for the stresses and pressure gradient. Similar reductions are possible in region C if $n = 1$. However, region A is more complicated, and the stresses and pressure must be found from solving the algebraic problem in (10), (14) and (16) (see also [27,4]). For the problems of interest, it is not known *a priori* where each type of flow field is attained (or if they appear at all); the relations in (10) and (14) encompass all four possibilities without having to explicitly identify the flow structure.

2.3. Force on surfaces

In the examples to follow, we also need to compute the forces on the moving surfaces in order to determine their dynamic evolution. To leading order in aspect ratio, the dimensional force per unit width acting on the lower surface due to the fluid is

$$\frac{\mathcal{L}^2\mathcal{T}}{\mathcal{H}} \int_D \left[\frac{\mathcal{H}}{\mathcal{L}}(\tau_1 + pY_{1x})\hat{\mathbf{x}} - p\hat{\mathbf{y}}\right] \mathrm{d}x. \tag{19}$$

Note that the force along the slot is much less than transverse to it. Also, because the fluid has no inertia, the force on the upper surface is equal and opposite to that on the lower surface.

3. Viscoplastic journal bearings

3.1. Bearings with prescribed motion

The journal bearing consists of an inner cylinder of dimensional radius a that is able to translate and rotate, contained within a stationary outer cylinder of dimensional radius b. We define the characteristic length scales, $\mathcal{H}$ and $\mathcal{L}$, by $\mathcal{H} = b - a$ and $\mathcal{L} = a$. In the laboratory frame, the dimensional position of the inner cylinder centre is

$$(b-a)\varepsilon(\cos\Theta, -\sin\Theta), \tag{20}$$

where the dimensionless separation of the two centres is $\varepsilon(t)$. The line of centres makes a clockwise-increasing angle $\Theta(t)$ with the horizontal (see the sketch in Fig. 2), and the inner cylinder's (dimensionless) rotation rate is $\Omega(t)$. We define x and y in terms of a clockwise polar (r,θ)-coordinate system centred on the inner cylinder and orientated by the line of centres (with $\theta = 0$ aligned with the narrowest part of the gap):

$$y = \frac{r-a}{b-a}, \qquad x = \theta. \tag{21}$$

The locations of the cylinder surfaces are therefore

$$Y_1 = 0 \quad \text{and} \quad Y_2 = 1 - \varepsilon\cos\theta. \tag{22}$$

and the fluid velocities are, to leading order,

$$U_1 = \Omega - \dot{\Theta}, \quad V_1 = 0, \tag{23}$$

$$U_2 = -\dot{\Theta}, \quad V_2 = -\dot{\varepsilon}\cos\theta - \varepsilon\dot{\Theta}\sin\theta. \tag{24}$$

Hence

$$h = 1 - \varepsilon\cos\theta, \quad U = -\Omega, \quad q = \frac{1}{2}h(\Omega - 2\dot{\Theta}) - \dot{\varepsilon}\sin\theta. \tag{25}$$

Finally, the bearing is periodic in θ, so $P = 0$ in (16).

A sample journal bearing solution, for prescribed geometry and cylinder velocity and rotation is shown in Fig. 4. This solution contains a fully yielded gap over two angular ranges (region C), two unconnected central pseudo-plugs (A), and genuine rigid zones attached to either cylinder (B and D). These flow morphologies become spliced together to create the overall flow pattern.

3.2. Small motions; large yield stress

For either large yield stress, $B \gg 1$, or small motions of the inner cylinder, $(\dot{\varepsilon}, \dot{\Theta}, \Omega, q, Q) \sim U \ll 1$, it becomes possible to calculate the flow field largely analytically. In these limits, the arrangement of alternating plugs, pseudo-plugs and yielded zones converges to certain patterns, as illustrated in Figs. 5 and 6. Notably, for the first example, $\tau_j \sim B$ over pairs of B,C and D regions, but there are intervening A regions in which the surface stresses have opposite sign with $|\tau_j| \sim B$. In the second example, $\tau_j \sim B$, throughout the gap and there are no pseudo-plugs.

Referring to the analysis of the different regions in Appendix B, we see that in the limit of large B or small U, the pressure gradient is

$$p_\theta = \frac{\tau_2 - \tau_1}{h} \sim \frac{2Bs_2}{h} \tag{26}$$

over region A and smaller elsewhere (except for the slender connection zones in regions B and D bordering region A). Thus, provided

Please cite this article in press as: I.J. Hewitt, N.J. Balmforth, Viscoplastic lubrication theory with application to bearings and the washboard instability of a planing plate, J. Non-Newtonian Fluid Mech. (2012), doi:10.1016/j.jnnfm.2011.11.008

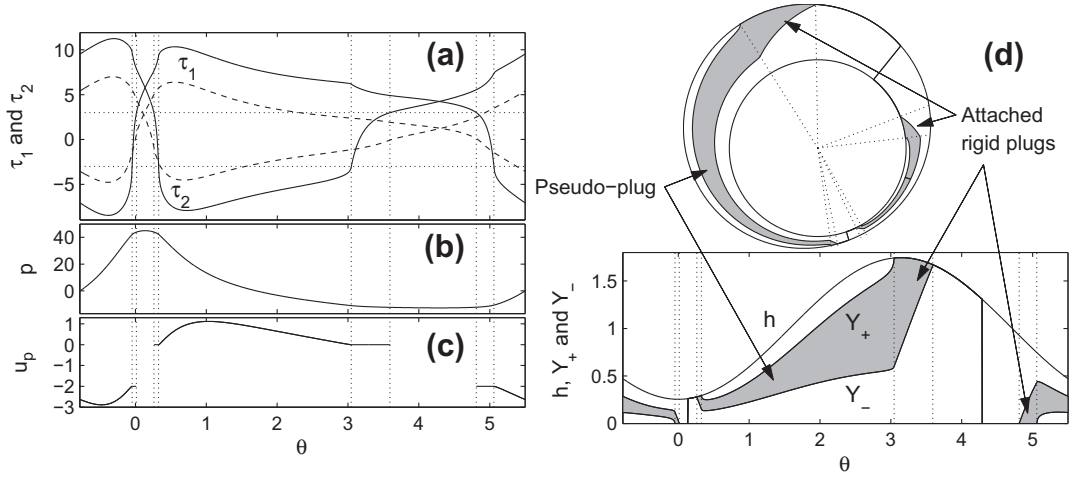

Fig. 4. A journal bearing solution, showing (a) τ_1 and τ_2, (b) p, (c) the plug speed u_p, and (d) h and $Y_\pm$ (either against θ or on a polar plot, with the plugs and pseudo-plugs shaded). The dashed curves in (a) show the Newtonian solution and the horizontal dotted lines show $\pm B$. The vertical and radial dotted lines show the borders of the various regions composing the overall flow pattern. Parameters are $\varepsilon = 0.745,\ \Theta = 1.11,\ \dot{\varepsilon} = 1,\ \Omega = -2,\ \dot{\Theta} = 0,\ n = \frac{1}{2}$ and $B = 3$, with $b - a = \frac{3}{8}a$ adopted for illustration.

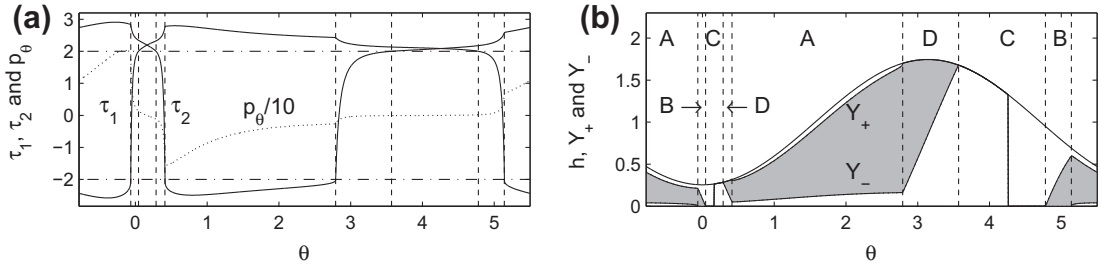

Fig. 5. A journal bearing solution with low speeds and rotation, showing (a) τ_1, τ_2 (both solid) and $p_\theta/10$ (dotted), and (b) h and $Y_\pm$ (with the plugs and pseudo-plugs shaded), for $\varepsilon = 0.745,\ \Theta = 1.11,\ \dot{\varepsilon} = 0.005,\ \Omega = -0.01,\ \dot{\Theta} = 0, n = \frac{1}{2}$ and $B = 2$.

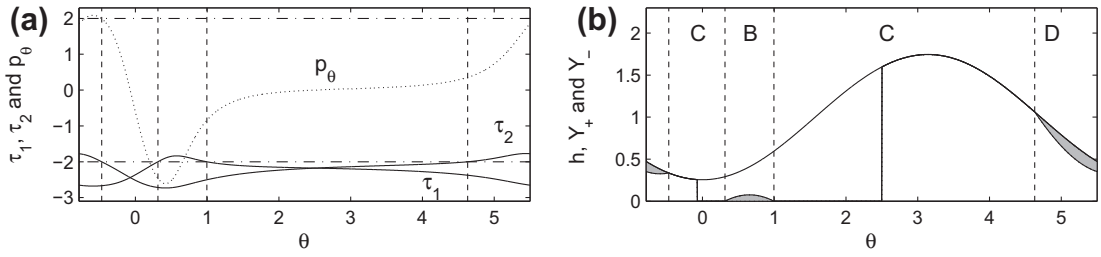

Fig. 6. A journal bearing solution similar to that in Fig. 5, but with $\varepsilon = 0.745,\ \Theta = \pi,\ \dot{\varepsilon} = 0.01,\ \Omega = 0.05$ and $\dot{\Theta} = 0.02$.

the flow pattern contains A regions as in Fig. 5, the periodicity condition, $\int_0^{2\pi} p_\theta \mathrm{d}\theta = 0$, is dominated by them and is equivalent, to leading order, to

$$\int_{\mathrm{A^B}} \frac{\mathrm{d}\theta}{h} = \int_{\mathrm{A^D}} \frac{\mathrm{d}\theta}{h}, \tag{27}$$

where $\mathrm{A^B}$ and $\mathrm{A^D}$ denote the two A regions that exist within the domain, which cover the angular intervals, $\left(\theta_{AB}^{(1)}, \theta_{AB}^{(2)}\right)$ and $\left(\theta_{AD}^{(1)}, \theta_{AD}^{(2)}\right)$, and are bordered by the B and D regions, respectively.[1] That is,

$$\left[\tan^{-1}\sqrt{\frac{1+\varepsilon}{1-\varepsilon}}\tan\frac{\theta}{2}\right]_{\theta_{AB}^{(1)}}^{\theta_{AB}^{(2)}} = \left[\tan^{-1}\sqrt{\frac{1+\varepsilon}{1-\varepsilon}}\tan\frac{\theta}{2}\right]_{\theta_{AD}^{(1)}}^{\theta_{AD}^{(2)}}. \tag{28}$$

Importantly, the borders of the A regions, $\theta_{AB}^{(k)}$ and $\theta_{AD}^{(k)}$ for $k = 1$ and 2, turn out to depend only on the velocity and rotation rate of the inner cylinder and Q (see (B.24)). Thus, (28) implicitly determines Q independently of the yield stress, and we find that

$$Q \sim \left(\frac{1}{2}\Omega - \dot{\Theta}\right)(1 - \varepsilon^2). \tag{29}$$

The most straightforward way to verify this limiting flux is to insert (29) into the relations specifying the edges of the A region (see Appendix B), solve them for $\theta_{AB}^{(k)}$ and $\theta_{AD}^{(k)}$, and then check that (28) is satisfied.

For later use we also quote the leading-order forms of the integrals,

$$f_\varepsilon = \int_0^{2\pi} p_\theta \sin\theta \ \mathrm{d}\theta \sim \frac{2Bs}{\varepsilon} \log\left[\frac{h\left(\theta_{AB}^{(2)}\right)h\left(\theta_{AD}^{(1)}\right)}{h\left(\theta_{AB}^{(1)}\right)h\left(\theta_{AD}^{(2)}\right)}\right], \tag{30}$$

$$f_\chi = -\int_0^{2\pi} p_\theta \cos\theta \ \mathrm{d}\theta \sim \frac{2Bs}{\varepsilon}\left[\theta_{AD}^{(1)} - \theta_{AD}^{(2)} + \theta_{AB}^{(2)} - \theta_{AB}^{(1)}\right], \tag{31}$$

[1] The connection zones within regions B and D, over which one of the surface stresses transitions from B to $-B$, or vice versa, and p_θ drops sharply from its value in (26), are too slender to contribute to the integral of p_θ to leading order.

Please cite this article in press as: I.J. Hewitt, N.J. Balmforth, Viscoplastic lubrication theory with application to bearings and the washboard instability of a planing plate, J. Non-Newtonian Fluid Mech. (2012), doi:10.1016/j.jnnfm.2011.11.008

and

$$T_f = \int_0^{2\pi} \tau_1 \, \mathrm{d}\theta \sim 2Bs\left[\pi + \theta_{AB}^{(1)} - \theta_{AB}^{(2)}\right], \tag{32}$$

where s is the sign of τ_1 over the A^D region. These limits follow from (26) and the leading-order forms of τ_1 in the various regions (over most of the A^D, B, C and D, we have $\tau_1 \sim Bs$, whereas $\tau_1 \sim -Bs$ over the A^B region).

These limits of the flux, forces and torque are rather different if the flow pattern does not contain any A regions, as in the second example of Fig. 6. In fact, for this case, Q, $|\tau_j| - B$, $Y_\pm$ and p_θ all become independent of B. This feature arises because the surface stresses become single-signed and B then cancels out from (10) and (14) (as can be shown with a little algebra; see Appendix B). Although the formulae for the pressure gradient simplify in this instance, the entire gap contributes to (16) and the flux constraint reduces to a relatively opaque implicit equation for Q (*cf.* [13]), preventing us from offering any concise limiting solutions.

3.3. Dynamic evolution

The leading-order force on the inner cylinder, which acts in the y-direction, is expressible in terms of the two unit vectors, $\hat{\boldsymbol{\varepsilon}}$ and $\hat{\boldsymbol{\chi}}$, directed along the line of centres (from the outer's centre to the inner's), and perpendicular to that line (in the counter-clockwise sense), since $\hat{\boldsymbol{y}} \equiv -\hat{\boldsymbol{\varepsilon}}\cos\theta - \hat{\boldsymbol{\chi}}\sin\theta$. Per unit width, the force is

$$\frac{\rho v a^2 \mathcal{U}}{(b-a)^2}(f_\varepsilon \hat{\boldsymbol{\varepsilon}} + f_\chi \hat{\boldsymbol{\chi}}) \equiv -\frac{\rho v a^2 \mathcal{U}}{(b-a)^2}\int_0^{2\pi} p(\hat{\boldsymbol{\varepsilon}}\cos\theta + \hat{\boldsymbol{\chi}}\sin\theta)\mathrm{d}\theta. \tag{33}$$

Furthermore, the clockwise torque per unit width acting on the inner cylinder, about its centre, is

$$\frac{\rho v a^2 \mathcal{U}}{(b-a)} T_f \equiv \frac{\rho v a^2 \mathcal{U}}{(b-a)}\int_0^{2\pi} \tau_1 \, \mathrm{d}\theta. \tag{34}$$

The equations of motion of the inner cylinder, subject to an external load, $-(\rho v a^2 \mathcal{U})/(b-a)^2$, acting vertically downwards, and a clockwise torque, $\rho v a^2 \mathcal{U} T/(b-a)$, each per unit length, are

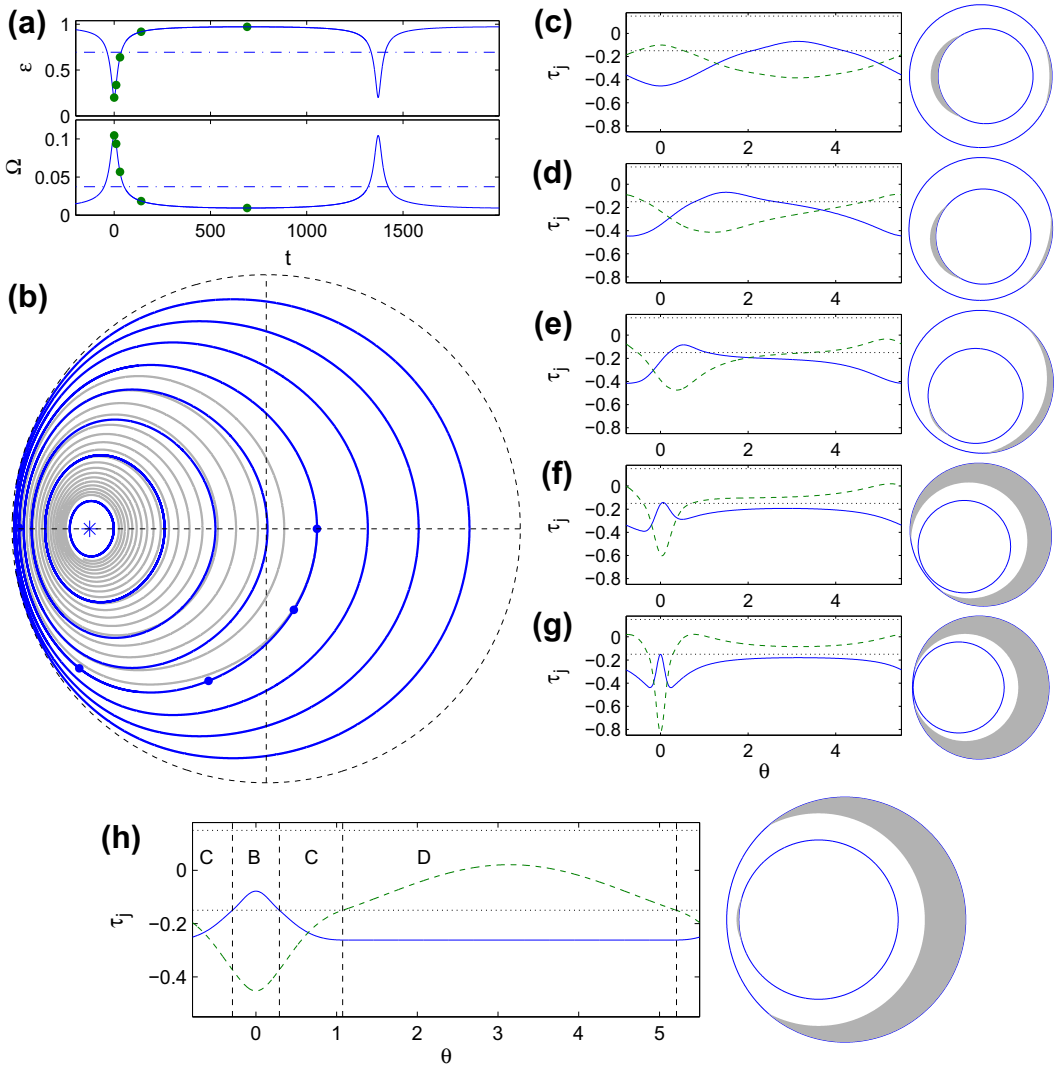

Fig. 7. Solutions of the inertialess initial-value problem ($\mathcal{I} = \mathcal{M} = 0$) for $T = 1.5$, $n = 1$ and $B = 0.15$. (a) show time series of ε and Ω for a solution starting at $\varepsilon = 0.2$ and $\Theta = 0$; the dot-dashed lines indicate the Sommerfeld equilibrium (ε_s, Ω_s). (b) shows a phase portrait of the evolving solution on the polar (ε, Θ)-plane, along with more solutions starting along the horizontal line through the outer cylinder centre. The dots indicate the times at which the snapshots of the surface stresses, τ_1 (solid) and τ_2 (dashed) are shown in (c)–(g) (the dotted lines indicate $\pm B$); the polar plots on the right display the position of the inner cylinder and the plug regions in the fluid gap are shaded ($b - a = 0.5a$ is adopted for illustration). In (b), the lighter grey line shows a solution with $\mathcal{I} = 50$ that spirals into the fixed point corresponding to the Sommerfeld equilibrium. Panel (h) shows the stresses and plug regions for that equilibrium; the rigid plug attached to the outer cylinder has constant radius (see Appendix B).

Please cite this article in press as: I.J. Hewitt, N.J. Balmforth, Viscoplastic lubrication theory with application to bearings and the washboard instability of a planing plate, J. Non-Newtonian Fluid Mech. (2012), doi:10.1016/j.jnnfm.2011.11.008

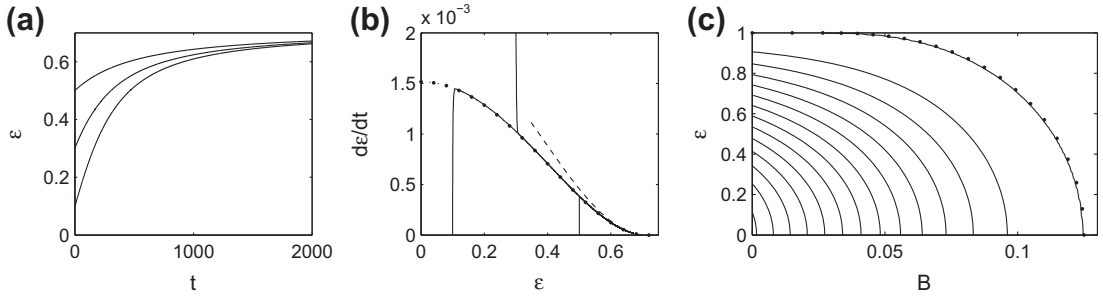

Fig. 8. Sedimentation solutions ($\Theta = \pi/2$ and $\Omega = T = 0$). (a) and (b) show solutions with $(\varepsilon(0), \dot{\varepsilon}(0)) = (0.1, 0),\ (0.3, 2\times10^{-3})$ and (0.5,0), for $n = 1$, $B = 0.1$ and $\mathcal{M} = 100$. The dotted line in (b) shows the solution for $\mathcal{M} = 0$ and the dashed line indicates the limiting $t \gg 1$ solution in (42). Panel (c) shows contours of constant $\dot{\varepsilon}$ on the (B,ε) − plane for $\mathcal{M} = 0$, in increments of 2×10^{-3}, starting at 10^{-6}; the dots show the curve $\varepsilon = \varepsilon_*(B)$ given by (43).

therefore

$$\mathcal{M}(\ddot{\varepsilon} - \varepsilon\dot{\Theta}^2) = f_\varepsilon + \sin\Theta,$$
$$\mathcal{M}(\varepsilon\ddot{\Theta} + 2\dot{\varepsilon}\dot{\Theta}) = f_\chi + \cos\Theta, \tag{35}$$
$$\mathcal{I}\dot{\Omega} = T_f + T,$$

where

$$\mathcal{M} = \mathrm{Re}\frac{m(b-a)^2}{\rho a^4}, \quad \mathcal{I} = \frac{I}{\rho a^4}\mathrm{Re}, \tag{36}$$

ρ is the fluid density and m and I are the inertial mass and moment of inertia per unit width of the inner cylinder, respectively ($\mathrm{Re} = \mathcal{U}(b-a)/\nu$). Note that we have exploited the speed scale $\mathcal{U}$, which is unspecified if the motion evolves dynamically, to scale the dimensionless imposed load to unity. Lastly, in lubrication theory, the reduced Reynolds number $\mathcal{H}\mathrm{Re}/\mathcal{L}$ is assumed small. Thus, in practice, if all the mass of the inner cylinder is contained within the bearing (implying $m = \pi a^2\rho_s$ and $I = ma^2/2$, with ρ_s the solid density) then it is likely that $\mathcal{M} \ll 1$. On the other hand, $\mathcal{I}$ may be order one (for moderate density ratios).

If the inertia of the inner cylinder is unimportant (the case usually considered for Newtonian journal bearings, see [1]), then $(\mathcal{M},\mathcal{I}) \to 0$ and the equations of motion (35) become implicit equations for the cylinder's radial and angular speeds, $\dot{\varepsilon}$ and $\dot{\Theta}$, and its rotation rate, Ω. These implicit equations can be solved by extending the Newton iteration algorithm described in Appendix A, and the ODEs then integrated in time. Sample solutions are shown in Fig. 7. The solution shown in detail corresponds to a periodic orbit in which the inner cylinder circulates inside the outer one, with plug zones adjacent to the walls expanding and shrinking as the inner cylinder shifts off-centre. Note that the dynamical system is non-dissipative in the inertia-less limit and the periodic orbit executed depends on the initial condition, just as for the Newtonian (full) journal bearing [1]. With rotational inertia ($\mathcal{I} > 0$), the system becomes dissipative, and the solution converges to the fixed point with $(\varepsilon,\Theta,\Omega) = (\varepsilon_s,\pi,\Omega_s)$, where the radial position, ε_s, and rotation rate, Ω_s, depend upon the yield stress. This fixed point is the analogue of the classical Sommerfeld solution, and is also shown in Fig. 7. Sommerfeld-type solutions without pseudo-plugs have been constructed previously for Bingham fluids [3,1,13].

3.4. Pure sedimentation

When there is no imposed torque ($T = 0$) and the inner cylinder begins without rotation ($\Omega(0) = 0$) from a position that is shifted off-centre in the direction of the imposed load ($\Theta(0) = \pi/2$), then that object "sediments" (a terminology more suitable when the load is gravity) without adjusting its angle or starting to rotate. The only nontrivial equation of motion is

$$\mathcal{M}\ddot{\varepsilon} = f_\varepsilon + 1. \tag{37}$$

Moreover, the symmetry of the problem demands that $\tau_1 = -\tau_2 = -hp_\theta/2$, $Y_+ = h - Y_-$, $U = Q = 0$ and $q = -\dot{\varepsilon}\sin\theta$, implying, from (14), that the stress τ_2 satisfies the algebraic equation,

$$\frac{h^2 I_1(\tau_2)}{2\tau_2^2} + \dot{\varepsilon}\sin\theta = 0. \tag{38}$$

The solution must then be fed into the integral f_ε (*cf.* (33)) in order that (37) can be integrated.

Sample numerical solutions for sedimentation are shown in Fig. 8. A key feature of these solutions is that the inner cylinder only sediments if the yield stress is sufficiently small: $B < \frac{1}{8}$. Moreover, even if $B < \frac{1}{8}$, the cylinder stops sedimenting and reaches an equilibrium position, $\varepsilon = \varepsilon_*(B) < 1$, without making contact with the outer cylinder.

To understand this dynamics, we first explore the limit, $B \to 0$ (*i.e.* a power-law fluid), for which $I_1(\tau_2) \to n|\tau_2|^{2+1/n}/(2n+1)\mathrm{sgn}(\tau_2)$. The resulting stress distribution indicates that $\varepsilon \to 1 - O(t^{-2})$ for $t \to \infty$, and as the inner cylinder approaches contact with the outer, the pressure over the narrowest part of the intervening gap dominates the resisting force. Hence

$$\tau_2 = -\left[\frac{2(2n+1)}{nh^2}\right]^n |\dot{\varepsilon}\sin\theta|^n \mathrm{sgn}(\dot{\varepsilon}\sin\theta)$$
$$\sim -2^n(2+1/n)^n\delta^{-3n}\frac{|\dot{\varepsilon}\Phi|^n\ \mathrm{sgn}(\Phi)}{(1+\Phi^2/2)^{2n}}, \tag{39}$$

for $\varepsilon = 1 - \delta^2$, $\theta = \delta\Phi$ and $h \sim \delta^2(1+\Phi^2/2)$ with $\Phi = O(1)$. The surface shear rate in the gap, $|u_y| = |\tau_2|^{1/n}$, is therefore of order $\dot{\varepsilon}\delta^{-3} = O(1)$ for $t \gg 1$. More importantly, the stresses and shear rate decline as one progresses outside the gap (i.e. for $|\Phi| \gg 1$): $\tau_2 \to |\Phi|^{-3n}$ and $|u_y| \sim |\Phi|^{-3}$. These observations suggest that, if the yield stress is reintroduced into the problem, the narrowest part of the gap is likely to remain yielded if so to begin with, but yield stresses will eventually dominate throughout the bulk of the gap elsewhere, thereby bringing the inner cylinder to rest before it makes contact.[2]

To proceed a little further, we consider the limit $\dot{\varepsilon} \ll 1$ in (38), which indicates that

$$1 \gg \frac{2\dot{\varepsilon}\tau_2^2}{h^2}\sin\theta = -I_1(\tau_2) \sim -\frac{nB}{n+1}(|\tau_2| - B)^{1+1/n}\mathrm{sgn}(\tau_2). \tag{40}$$

[2] The same considerations apply to the more classical problem of the sedimentation of a smooth object towards a plane surface through a viscous fluid (*e.g.* [19]). That is, the Newtonian solution predicts $O(1)$ shear rates within the narrowest parts of the intervening gap, where the lubrication pressure is highest, but increasingly low shear rates elsewhere. Thus sedimentation in a yield-stress fluid is controlled by yield stresses outside the narrowest part of the gap. Such a situation defies straightforward analysis in general geometries (*cf.* [17]) but remains analytically accessible in the geometry of the journal bearing.

Please cite this article in press as: I.J. Hewitt, N.J. Balmforth, Viscoplastic lubrication theory with application to bearings and the washboard instability of a planing plate, J. Non-Newtonian Fluid Mech. (2012), doi:10.1016/j.jnnfm.2011.11.008

Hence, to leading order (given that $\tau_2 = \frac{1}{2}hp_\theta$)

$$p_\theta \sim -\left\{\frac{2B}{h} + \frac{2}{h}\left[\frac{2\dot\varepsilon B(n+1)}{nh^2}|\sin\theta|\right]^{n/(n+1)}\right\}\mathrm{sgn}(\sin\theta). \tag{41}$$

Finally, ignoring the inertial term in (37) (which is small in this limit), we arrive at the force balance

$$2\dot\varepsilon B\frac{n+1}{n}\left[4\int_0^\pi \frac{(\sin\theta)^{(2n+1)/(n+1)}\,\mathrm{d}\theta}{(1-\varepsilon\cos\theta)^{(3n+1)/(n+1)}}\right]^{(n+1)/n} \sim \left[1-\frac{4B}{\varepsilon}\log\left(\frac{1+\varepsilon}{1-\varepsilon}\right)\right]^{(n+1)/n}. \tag{42}$$

The inner cylinder therefore comes to rest as $\varepsilon \to \varepsilon_* - O(t^{-1/n})$, where

$$1 = \frac{4B}{\varepsilon_*}\log\left(\frac{1+\varepsilon_*}{1-\varepsilon_*}\right). \tag{43}$$

The predictions in (42) and (43) are also shown in Fig. 8. Note that the final $O(t^{-1/n})$ approach to rest is relatively slow and coincides with the convergence to the final shapes encountered for the slumps of free surface flows [28], and is quite different from the finite stopping time found for confined flows with fixed boundaries (*e.g.* [29]).

3.5. General stopping conditions

The relation in (43) provides the radial location along the midline of the bearing ($\Theta = \pi/2$) at which the inner cylinder is brought to rest if $B < \frac{1}{8}$. We may arrive at this condition more directly, and also generalize it to arbitrary positions and rotations, by considering the limits of the forces implied by (30)–(32), in tandem with the equations of motion (35) with the inertial terms neglected. For simplicity, we describe the analysis explicitly assuming that the cylinder is not able to rotate at all, so that $\Omega = 0$. In this case, the B, C and D regions all shrink to zero width (indicating that there are sharp jumps in the surface shear stresses, τ_1 and τ_2, across the borders of the two A regions; *cf.* Fig. 9(c)) and $\theta_{AD}^{(2)} \to \theta_{AB}^{(1)}$ and $\theta_{AD}^{(1)} \to \theta_{AB}^{(2)} + 2\pi$, after arranging the domain so that A^D always lies to the left of A^B. Thus

$$\frac{4B}{\varepsilon}\ln\left[\frac{h\left(\theta_{AB}^{(1)}\right)}{h\left(\theta_{AB}^{(2)}\right)}\right] \approx \sin\Theta, \qquad \frac{4B}{\varepsilon}\left[\pi - \theta_{AB}^{(2)} + \theta_{AB}^{(1)}\right] \approx \cos\Theta. \tag{44}$$

If we set $\dot\Theta = \Upsilon\dot\varepsilon$, and recall from (29) that $Q \to -(1-\varepsilon^2)\dot\Theta$ in this limit, we may determine the critical values of Υ and B for which the inner cylinder is brought to rest at the position $(\varepsilon,\Theta) = (\varepsilon_*,\Theta_*)$. The critical value of Υ is given only implicitly by (44), and it is more expedient to compute Θ_* and B explicitly from (44), given values for ε_* and Υ (and first determining $\theta_{AB}^{(k)}$ from (B.24)); see Fig. 9. This figure also reports the results of some initial-value computations that illustrate the convergence to the stopping condition for $B = 0.1$. For $\Theta_* = \pi/2$, $\Upsilon = 0$ and (44) reduce to (43); conversely, for $\Theta_* \to 0$, $\Upsilon \to \infty$ and we discover $B = \varepsilon_*/(4\pi - 8\cos^{-1}\varepsilon_*)$. For $B < 1/4\pi$, the curves representing the stopping condition intersect the outer cylinder at a given angle, Θ, suggesting that the inner cylinder can either sediment onto the outer wall or be brought to rest inside the bearing, depending on the path taken from the initial condition.

If the inner cylinder also rotates under an imposed torque, then the stopping conditions must necessarily change. If the torque sets a given rotation rate, then the fluid must yield to accommodate the imposed shear; the inner cylinder then always sediments onto the outer cylinder unless the rotation is sufficient to suspend it indefinitely, as in the sample solutions shown in Fig. 7. On the other hand, if the torque is fixed, then it is possible that the inner cylinder simultaneously comes to rest and stops rotating; the corresponding stopping criterion can be determined much as above, though with more effort, assuming that the dynamics is controlled by the A regions present in the flow pattern. Awkwardly, those regions actually disappear if the torque and rotation rate become too large, calling for a different asymptotic description. We avoid becoming overly distracted by such technical detail, and now move on to our second lubrication problem.

4. Viscoplastic sliders, blades and washboards

We next consider an inclined plate moving over the surface of a viscoplastic layer, as sketched in Fig. 2c. The plate is held at a constant angle α to the horizontal and moves with a fixed horizon-

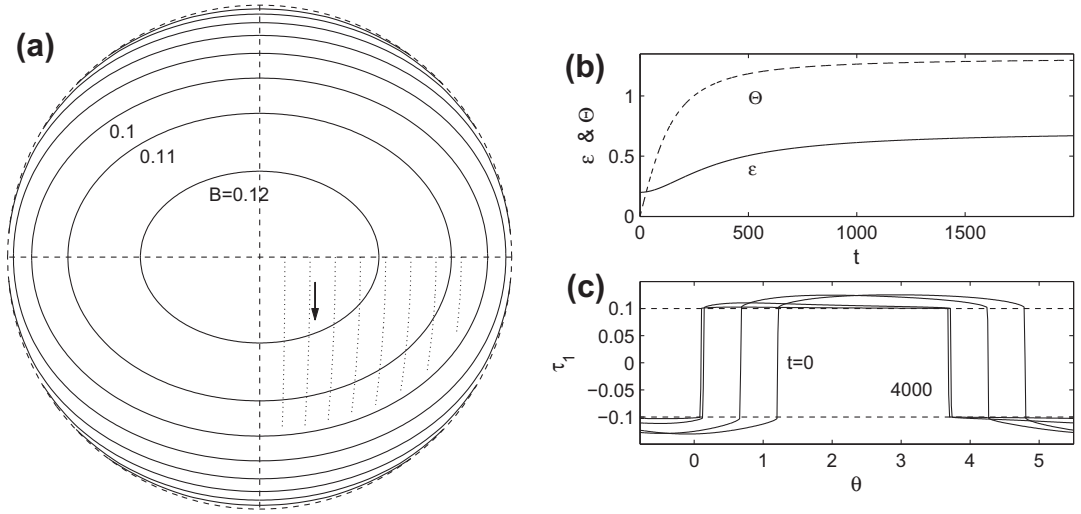

Fig. 9. (a) Stopping conditions for $\Omega = 0$; shown are polar plots of the critical curves, $[\varepsilon_*(B),\Theta_*(B)]$, for $B = 0.05, 0.06, \ldots, 0.12$. The dotted lines show phase portraits on the same polar plane of inertialess initial-value problems with $[\varepsilon(0),\Theta(0)] = (0.1k, 0)$, for $B = 0.1$ and $k = 1, 2, \ldots, 8$, all with the same duration ($t < 4000$). Further details of the initial-value computation with $\varepsilon(0) = 0.2$ are shown in the other two panels: (b) shows the time series of $\varepsilon(t)$ and $\Theta(t)$, and (c) shows snapshots of $\tau_1 = -\tau_2$ at the times $t = 0$, 100, 1000 and 4000 (the dashed lines denote $\pm B$).

Please cite this article in press as: I.J. Hewitt, N.J. Balmforth, Viscoplastic lubrication theory with application to bearings and the washboard instability of a planing plate, J. Non-Newtonian Fluid Mech. (2012), doi:10.1016/j.jnnfm.2011.11.008

tal speed $\mathcal{U}$. We will work in a frame that moves horizontally with the plate, for which the lowest point (the 'tip') lies at $x = 0$ and $y = Y(t)$; the plate moves vertically with speed $\dot{Y}$. On selecting $\mathcal{H}/\mathcal{L} = \tan\alpha$ in the non-dimensionalization of Section 2, the surfaces confining the fluid gap are given by

$$Y_1 = 0, \quad Y_2 = Y + x, \tag{45}$$

and the velocities there are

$$\begin{pmatrix} U_1 \\ V_1 \end{pmatrix} = \begin{pmatrix} -1 \\ 0 \end{pmatrix}, \quad \begin{pmatrix} U_2 \\ V_2 \end{pmatrix} = \begin{pmatrix} 0 \\ \dot{Y} \end{pmatrix}. \tag{46}$$

Hence, in the notation of Section 2

$$h = Y + x, \quad U = 1, \quad q = -\frac{1}{2}h + \dot{Y}x. \tag{47}$$

The fluid makes contact with the plate over the section $0 \leqslant x \leqslant L$, and we impose $p = 0$ at the two ends, implying $P = 0$ in (16). The dimensionless lift force on the plate due to the fluid is

$$f(Y, \dot{Y}, L; B) = \int_0^L p \, dx, \tag{48}$$

written to emphasize the parametric dependence on the yield stress, which is one of our main objectives below. Hereon, we also focus on the Bingham fluid ($n = 1$), for which additional analytical headway is possible, expediting the exploration.

4.1. Slider bearing and blade coating solutions

The configuration summarized above applies to the classical lubrication problems of the slider bearing and blade coating [1,23]. For the slider bearing, the length L and the position of the upper surface Y are fixed, and one requires the forces on the plate. In blade coating, L and Y are again prescribed, but the flux, and therefore the depth of the fluid layer left behind are of primary interest. In either case, we may set $L = 1$, equivalent to a choice of horizontal lengthscale $\mathcal{L}$.

Fig. 10 shows how the lift force on a slider bearing varies with the size of the gap and the yield stress of the fluid. In the Newtonian case, the lift force is given by the standard expression

$$f_0(Y, L; 0) = 12\left[\frac{1}{2}\log\left(\frac{Y+L}{Y}\right) - \frac{L}{2Y+L}\right], \tag{49}$$

In the limit of large B, as shown in Appendix C (see also [1]), the force is instead given by

$$f_0(Y, L; \infty) = \begin{cases} 12\left[\frac{1}{2}\log\left(\frac{Y+L}{Y}\right) - \frac{L}{2Y+L}\right] & Y \geqslant L \\ \frac{1}{9}\left[\left(\frac{Y+L}{Y}\right)^2 - 2\log\left(\frac{Y+L}{Y}\right) + 56\log 2 - 40\right] & Y < L. \end{cases} \tag{50}$$

As seen in Fig. 10, $f_0(Y,L;B) \geqslant f_0(Y,L;0)$ for given Y. Note that $f_0(Y,L;B) = f_0(Y,L;\infty)$ for finite yield stress if

$$B \geqslant B_c(Y, L) = \frac{(2Y+L)}{9Y^3}(L - Y)_+. \tag{51}$$

The critical value, $B_c(Y,L)$, increases monotonically from 0 to ∞ as Y decreases from L to 0, and arises because of the disappearance of any pseudo-plugs (A regions) within the flow (see Appendix C). Note that if $Y \geqslant L$ the Newtonian expression (49) holds regardless of the value of B, since the fluid is always fully yielded in that case. In general, however, for $0 < B < B_c$, there is no analytical expression

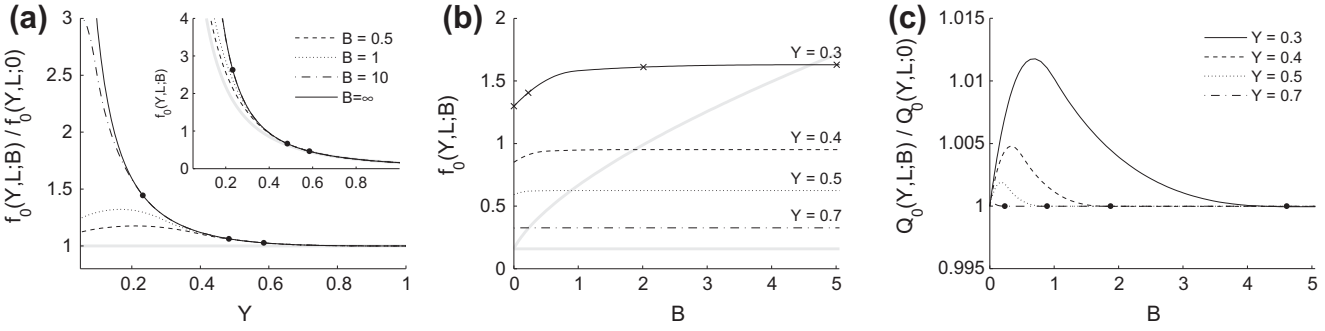

Fig. 10. Steady state relationships for gap width Y, lift force f_0, and yield stress B, with $L = 1$ for a Bingham fluid: (a) $f_0(Y,L;B)/f_0(Y,L;0)$ as a function of Y for the values of B indicated (the inset shows the actual forces $f_0(Y,L;B)$), (b) f_0 as a function of B for four different values of Y. The fluid is fully yielded below the lower grey line, has plugs attached to the upper and lower surfaces between the two grey lines, and has a central pseudo-plug above the upper grey line. Panel (c) shows $Q_0(Y,L;B)/Q_0(Y,L;0)$ as a function of B. Crosses in (b) mark the cases shown in Fig. 11. Dots on the curves in (a) and (c) mark the transition between states that involve pseudo-plugs and those that do not.

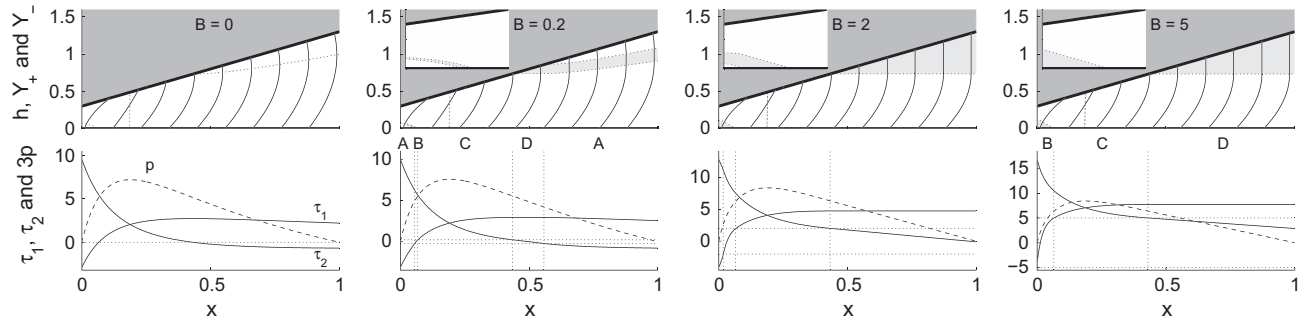

Fig. 11. Steady state flow configurations and stress distributions for the values of B indicated, with constant gap width $Y = 0.3$ and wetted length $L = 1$ (corresponding to the crosses in Fig. 10b). The top row shows flow profiles at nine locations along the gap; the lightly shaded regions indicate the plugs and pseudo-plugs (with insets showing magnifications near the trailing edge, $0 < x < 0.1$). In the bottom row, the horizontal dotted lines show $\pm B$.

Please cite this article in press as: I.J. Hewitt, N.J. Balmforth, Viscoplastic lubrication theory with application to bearings and the washboard instability of a planing plate, J. Non-Newtonian Fluid Mech. (2012), doi:10.1016/j.jnnfm.2011.11.008

for $f_0(Y,L;B)$, and the lift force must be computed numerically, using a method like that in Appendix A.

Fig. 11 shows sample solutions for the steady slider bearings, for different values of the yield stress. Provided $Y < L$ (as in these cases), the Newtonian solution possesses curves of zero shear stress which, when a small yield stress is added, broaden into pseudo-plugs (*i.e* region A; the overall arrangement of the flow pattern is A–B–C–D–A, see the second panel of Fig. 11). As the yield stress is increased, these pseudo-plugs thicken and turn into real plugs by becoming attached to the upper surface (region D) near the leading edge (third panel of Fig. 11), and to the lower surface (region B) near the trailing edge. The A region disappears entirely once the plugs are both fully attached to the surfaces for $B > B_c(Y,L)$; the flow structure then becomes independent of the yield stress and the sole effect of B is to shift the surface shear stresses (final panel of Fig. 11; the flow arrangement is now B–C–D). The yield surface within region D is conspicuously flat, a fact which is easily verified from the details in Appendix B, where with $q = -\frac{1}{2}h$ and $U = 1$, the stress τ_1, pressure gradient p_x and yield surface Y_- are all seen to be independent of x ((B.14)–(B.17)).

The horizontal drag force on the plate can also be calculated, and an analytical expression found for the case when there is no A region (see [1]). The force is dominated by the shear stresses for $B \gg 1$ (see (19)), and therefore increases linearly with B in this limit, whereas the vertical lift force becomes independent of B. On the other hand, the shear stress cannot continue to increase without bound in the lubrication analysis without violating the implicit assumption that this stress is smaller than the pressure by a factor of order of the aspect ratio; a different analysis is called for at such high yield stress.

Note that solutions equivalent to the final example of Fig. 11 were presented by Milne [3], but the flow pattern appears to have been assumed to take the relevant form, and the possibility that pseudo-plugs may exist for $B < B_c(Y,L)$ is not mentioned. Later work [1,27,4,30] notes the possibility, but does not provide any solutions with pseudo-plugs; thus, Figs. 10 and 11 provide a more complete summary of viscoplastic slider bearings.

For the blade coater, the steady flux $Q = Q_0(Y,L;B)$, determines the depth, η_T, of the layer of fluid emplaced downstream of the plate: by mass conservation, $\eta_T = -Q_0$. The classical Newtonian solution [31,23] gives the flux as

$$Q_0(Y,L;0) = -\frac{Y+L}{2Y+L}Y. \tag{52}$$

Thus, η_T varies from $\frac{1}{2}Y$ to Y as the gap becomes narrower. For finite yield stress, it turns out that $Q_0(Y,L;B) = Q_0(Y,L;0)$ provided the plugs are fully attached ($B \geqslant B_c(Y,L)$; see Appendix C). When there is an A region, for $0 < B < B_c(Y,L)$, the flux is slightly enhanced, $Q_0(Y,L;B)/Q_0(Y,L;0) > 1$, as shown in Fig. 10c.

4.2. Washboarding dynamics

For the washboard problem, the vertical position of the plate is not fixed, but adjusts in response to the downward load imposed on the plate and the fluid lift force. This demands that the wetted length, $L(t)$, also vary as fluid is dredged up from the incoming layer and pushed out upstream of the plate. Simultaneously, the fluid left behind becomes of variable depth, allowing for the possibility of a downstream flow adjustment. In principle, the full solution of the problem therefore requires us to consider the free-surface flows to either side of the plate, and match both to the flow underneath the plate. Unfortunately, for $x < 0$ and $x > L(t)$, the formulation of Section 2 no longer applies because we must now impose stress conditions at the upper surface, and, in principle, include surface tension and gravity. To simplify the situation, we neglect those effects, in which case lubrication theory predicts that the pressure and shear stress are both zero throughout the upstream and downstream layers owing to the stress-free surface conditions. Thus, as for the slider and blade solutions, the pressure still vanishes at the plate's edges and $P = 0$.

Upstream of the plate, the entire fluid layer is of uniform depth, $\mathcal{H}$, and moves with the velocity of the lower boundary, $-\mathcal{U}$ (*ie.* it is stationary in the frame of the fluid bed). These scales can be used for the non-dimensionalization of the problem, implying that the upstream solution has unit depth and speed $u = -1$. Underneath the plate, on the other hand, the flow takes a very different form, satisfying no slip on both surfaces, and the fluid depth at the leading edge, $h(L,t) = Y + L$, is not necessarily equal to unity. With a reintroduction of gravity and surface tension, free surface gradients drive flow that smoothes out any discontinuities, but because we neglect that physics, we must accept a jump in depth across the leading (and also trailing) edge of the plate. The effect of gravity in smoothing out this jump is discussed in Appendix D.

To connect the uniform upstream layer with the flow under the plate we apply a jump condition to conserve mass: for $x > L(t)$, there is a dimensional flux $-\mathcal{H}\mathcal{U}$, or a dimensionless flux of -1. On the other hand, for $x \to L(t)$ from the left, the (dimensionless) flux is $Q - L\dot{Y}$. Any difference in these two fluxes forces the wetted length to change and the fluid "wedge" underneath the plate to grow or shrink. The transport associated with the motion of the leading edge is $[h(L,t)-1]\dot{L}$, and so mass conservation demands $[h(L,t)-1]\dot{L} = Q - \dot{Y}L + 1$. That is,

$$(Y + L - 1)\dot{L} = Q + 1 - \dot{Y}L. \tag{53}$$

Behind the plate, the flow dynamics beneath that obstruction dictates the outflowing layer depth. Again, in the absence of surface tension and gravity, the free surface depth, $\eta(x,t)$, need not be the same as the height of the plate's tip at the trailing edge, but is determined by mass conservation: $\eta(0,t) \equiv \eta_T(t) = -Q(t)$, where η_T is the free surface depth just downstream of the trailing edge. In the moving frame of the plate, the free surface is simply advected downstream according to

$$\eta_t - \eta_x = 0, \quad \eta(0,t) = \eta_T(t), \tag{54}$$

with solution

$$\eta(x,t) = -Q(t+x). \tag{55}$$

If the elevation of the plate is fixed, we recover the blade-coating formula outlined earlier.

Finally, we write the equation of motion for the vertical position of the paddle:

$$\mathcal{M}\ddot{Y} = -\mathcal{W} + f, \quad f(Y,\dot{Y},L) = \int_0^L p \, \mathrm{d}x \tag{56}$$

(suppressing the parameterical dependence on B). In this dimensionless equation, the 'load' $\mathcal{W}$ corresponds to a dimensional weight, $\mathcal{W}\mathcal{L}^2\mathcal{T}/\mathcal{H}$, and $\mathcal{M}$ corresponds to a dimensional inertial mass, $\mathcal{M}\mathcal{L}^4\mathcal{T}/\mathcal{U}^2\mathcal{H}^2$ (if the weight is g times the inertial mass, then $\mathcal{W} = \mathcal{M}\,(g\mathcal{L}/\mathcal{U}^2)(\mathcal{L}/\mathcal{H})$).

To summarize: given current values of $Y, \dot{Y}$ and L, the algebraic Eqs. (10), (14) and (16) can be solved to determine the distribution of shear stresses and pressure gradient p_x beneath the plate, as well as the flux Q. This determines the lift force in (56), and completes the right-hand side of (53). That third-order system can then be integrated forwards in time. Our goal is to find planing states, where the plate is dragged steadily over the viscoplastic layer, and then explore whether these states are stable, or suffer an instability wherein the plate oscillates up and down, imprinting a washboard pattern on the surface left behind.

Note that a key simplification in the prescription is afforded when the flow pattern does not contain any pseudo-plugs (A re-

Please cite this article in press as: I.J. Hewitt, N.J. Balmforth, Viscoplastic lubrication theory with application to bearings and the washboard instability of a planing plate, J. Non-Newtonian Fluid Mech. (2012), doi:10.1016/j.jnnfm.2011.11.008

gions). In this situation, and as for the steady problems considered in Section 4.1, the formulae simplify sufficiently that the flux, Q, and lift force, $f(Y,\dot{Y},L)$, can be computed analytically. The details of this computation are outlined in Appendix C; importantly, both the force and flux become independent of the yield stress B.

4.3. Steady planing

The washboard Eqs. (53)–(56) admit a steady planing solution in which the vertical position Y and the wetted length L are tuned so that the lift force f balances the prescribed load $\mathcal{W}$, and the flux beneath the trailing edge Q matches the influx from upstream, -1. This exercise constitutes a nonlinear algebraic problem for the two unknowns, L and Y. In practice, however, it is more expedient to determine the steady state load, $f_0(Y;B)$ and wetted length, $L_0(Y;B)$, that are required for a given plate position Y.

Fig. 12 illustrates how such steady planing states depend upon the yield stress of the fluid, and Fig. 13 presents sample flow patterns. The results are qualitatively similar to those for the slider bearing or blade coater, the main difference being the determination of L from the flux condition, $Q=-1$. In the flow patterns of Fig. 13, the first case is fully yielded (region C alone), whereas the second example has pseudo-plugs at the leading and trailing edges (the arrangement is A-B-C-D-A); in the third example, the right-hand plug has attached to the plate and become truly rigid (arrangement A-B-C-D), and both plugs are attached to the two surfaces in the fourth example (arrangement B-C-D).

As before, any pseudo-plugs disappear when the yield stress exceeds the critical value in (51) (although L is not yet known), and the flux Q thereafter becomes equal to the Newtonian value in (52). In that case, $L_0(Y;B)=L_0(Y;0)$, with flux balance demanding

$$L_0(Y;0)=\frac{(2-Y)Y}{Y-1}. \tag{57}$$

The steady planing depth must therefore lie over the range $1\leqslant Y\leqslant 2$. With this wetted length, the critical yield stress (51) reduces to

$$B_c(Y)=\frac{(3-2Y)_+}{9(Y-1)^2}. \tag{58}$$

For $B\geqslant B_c$, the steady load required for the adopted Y is given by (50). If $Y\geqslant 3/2$ (equivalently, $L_0(Y;0)\leqslant Y$ or $f_0\leqslant 6\log 2-4$), the steady state is fully yielded regardless of the value of B and the load reduces to (49).

As seen in Fig. 12, as the yield stress is increased for a given plate height, the steady state load varies smoothly between the Newtonian value, $f_0(Y;0)$, and the large-B limit, $f_0(Y;\infty)$. At the same time, the wetted length first drops below $L(Y;0)$ before returning to that same value once the pseudo-plugs disappear.

4.4. Washboard instability

We now explore the stability of the planing states described above by solving the equations of motion as an initial-value problem. Some examples are shown in Figs. 14 and 15; in short, the steady planing state is stable when the imposed weight $\mathcal{W}$ is sufficiently large, but becomes unstable to vertical oscillations when $\mathcal{W}$ falls below a threshold value that depends upon the inertia $\mathcal{M}$ and the rheological properties.

When the steady planing state is unstable, the vertical oscillations of the plate amplify until a periodic oscillation is established. The amplitude of this oscillation increases as the load is reduced

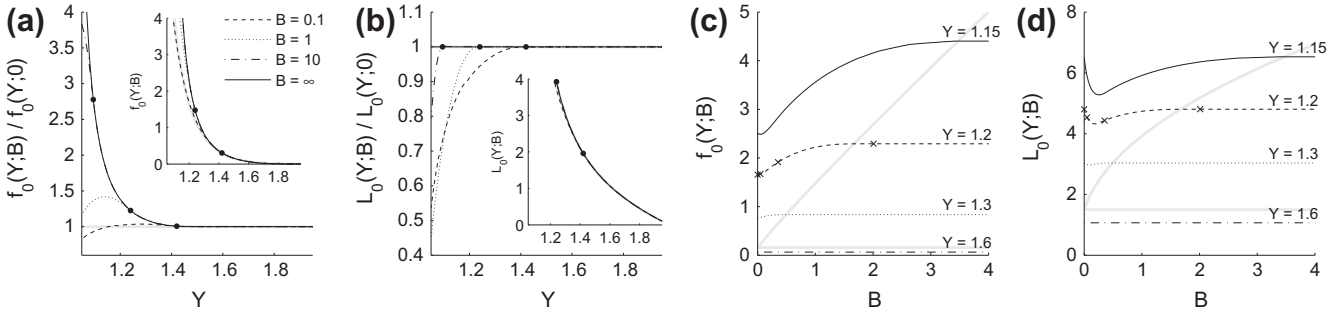

Fig. 12. Steady state planing relationships between plate height Y, lift force f_0, wetted length L_0, and yield stress B. Panels (a) and (b) show $f_0(Y;B)/f_0(Y;0)$ and $L_0(Y;B)/L_0(Y;0)$ as functions of Y for the yield stresses indicated. Panels (c) and (d) show f_0 and L_0 as functions of B for the values of Y indicated. Below the lower grey line the flow is fully yielded, between the two grey lines there are plugs attached to the upper and lower surfaces, and there is a central pseudo-plug above the upper grey line. Crosses in (c) and (d) mark the cases shown in Fig. 13. Dots on the curves in (a) and (b) mark the transition between states that involve pseudo-plugs and those that do not.

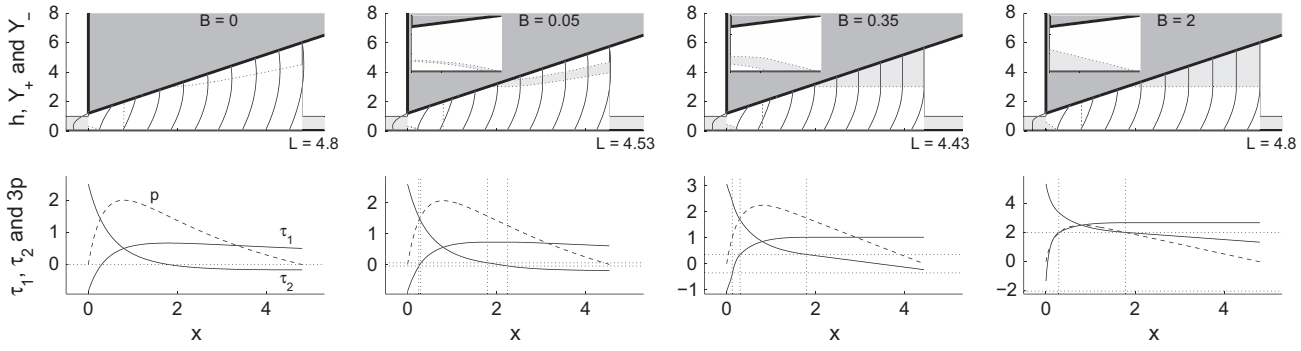

Fig. 13. Steady state flow patterns and stress distribution for the values of B indicated and $Y=1.2$ (corresponding to the crosses in Fig. 12). The top row shows flow profiles at ten locations along the gap; the lightly shaded regions indicate the plugs and pseudo-plugs (along with a magnification in the vicinity of the trailing edge, $0<x<0.3$). In the bottom row, the horizontal dotted lines show $\pm B$.

Please cite this article in press as: I.J. Hewitt, N.J. Balmforth, Viscoplastic lubrication theory with application to bearings and the washboard instability of a planing plate, J. Non-Newtonian Fluid Mech. (2012), doi:10.1016/j.jnnfm.2011.11.008

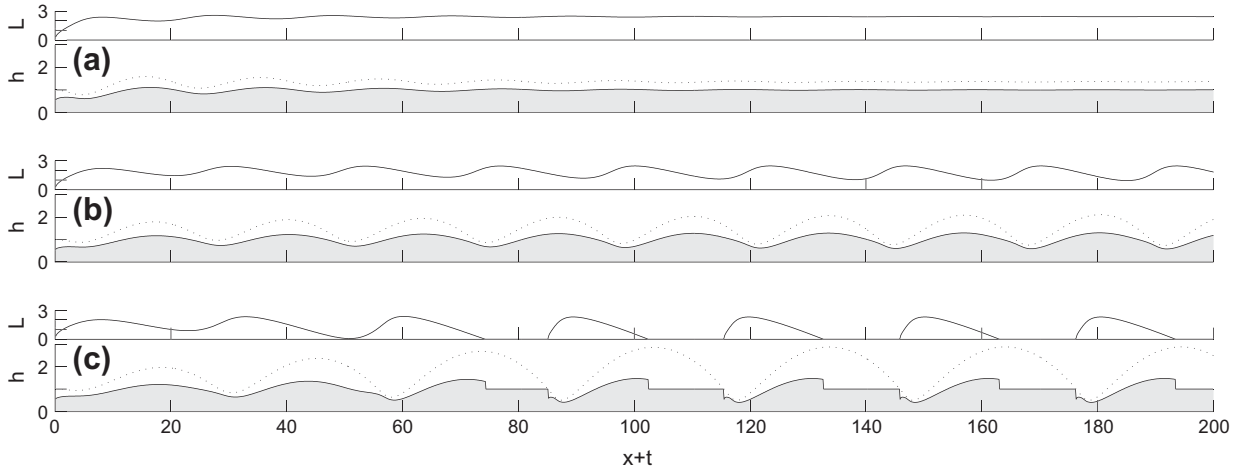

Fig. 14. Initial-value problems in which the plate begins at rest on the undisturbed surface of the fluid ($Y = 1, \dot{Y} = 0$ and $L = 0$ at $t = 0$) with weights of (a) $\mathcal{W} = 0.5$, (b) $\mathcal{W} = 0.35$ and (c) $\mathcal{W} = 0.25$. The shaded area shows the pattern imprinted on the fluid layer, the dotted line shows the trajectory of the plate tip, and the upper panels show the wetted length $L(t)$ during the motion. These are solutions for a Bingham fluid with large B, and $\mathcal{M} = 10$.

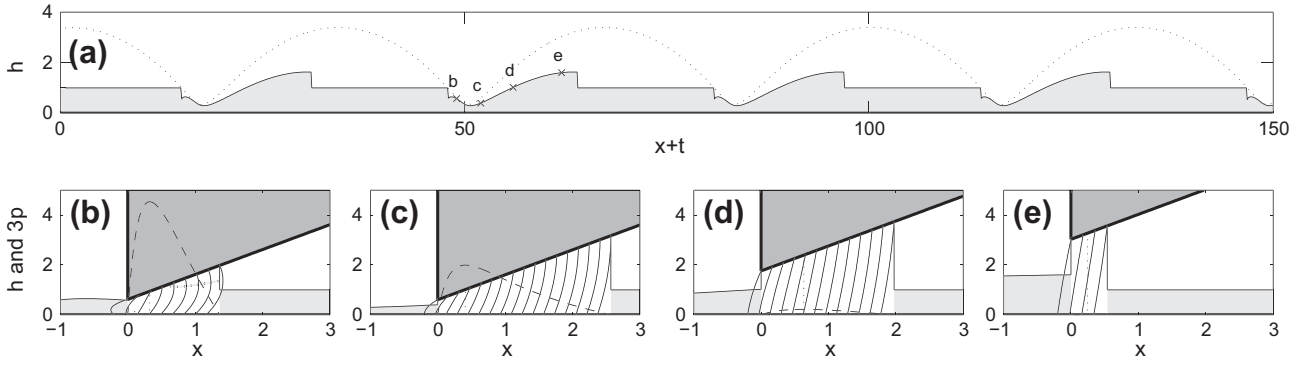

Fig. 15. A periodic oscillation for a Bingham fluid with $B = 0.05, \mathcal{M} = 10, \mathcal{W} = 0.26$. (a) shows the imprinted pattern (shaded) and the trajectory of the plate tip (dotted line). (b) shows snapshots of the flow profiles (solid lines) and pressure (dashed lines) at four times during one oscillation, as marked by crosses in (a).

(moving further from the stability threshold), and for sufficiently small weight the oscillations become strong enough that the plate loses contact with the fluid for part of the cycle (that is, the wetted length L vanishes over a fraction of the period). After taking off, the plate follows a ballistic trajectory, making contact with the fluid again when Y falls back to the undisturbed surface depth. Note how the plate's take off and landing deposit a cliff in the underlying fluid layer (an artifact of the lubrication approximation and our neglect of surface tension and gravity). This is because the flux Q at those instances is not equal to the undisturbed value -1; indeed in the case that there are no pseudo-plugs, one can show that $\eta_T = \frac{1}{2}Y$ at take-off and landing (when $L = 0$; see Appendix C and (C.3)).

Fig. 16a shows how the amplitude of the periodic states varies with the yield stress. As B is increased from zero, the threshold weight for instability is slightly reduced, but becomes independent of B once the yield stress exceeds a critical value corresponding to the disappearance of pseudo-plugs from the steady planing state. The amplitude of the oscillations continues to depend on B above this critical value, however, owing to the generation of such A regions during the unsteady oscillations. At sufficiently large B, the pseudo-plugs do not occur even during the oscillations, and the plate dynamics then becomes completely independent of B.

When there are no pseudo-plugs, an analytical expression is available for $f(Y, \dot{Y}, L)$ (see (C.4)–(C.6)). In such situations, it is straightforward to explore the linear stability; the condition for instability may be expressed as

$$\mathcal{W} < \mathcal{W}_*(\mathcal{M}; \infty), \tag{59}$$

with $\mathcal{W}_*(\mathcal{M}; \infty)$ shown in Fig. 16b. This condition also applies for any sufficiently large $B > B_c(Y)$ (Y being the steady state value corresponding to $\mathcal{W}_*$). A similar calculation for the Newtonian case indicates that instability occurs for $\mathcal{W} < \mathcal{W}_*(\mathcal{M}; 0)$, as also shown in Fig. 16b (note that for $\mathcal{W}_* < 6\log 2 - 4 \approx 0.159, B_c(Y) = 0$ so the two conditions are equal). For intermediate values of B the critical $\mathcal{W}_*(\mathcal{M}; B)$ must be determined numerically, and additional calculations suggest a monotonic variation between $\mathcal{W}_*(\mathcal{M}; 0)$ and $\mathcal{W}_*(\mathcal{M}; \infty)$.

4.5. Shape of the imprinted pattern

The washboarding theory above ignores the effects of gravity and surface tension on the fluid layer, and therefore places jumps in the height of the downstream layer when the plate lands and takes off. This free surface pattern becomes 'frozen' into the fluid, even if there is no yield stress. More realistically, gravity and surface tension smooth out the surface over the regions where the shear stresses generated by the surface slope and curvature exceed the yield stress (in the experimental images shown in Fig. 1, the

Please cite this article in press as: I.J. Hewitt, N.J. Balmforth, Viscoplastic lubrication theory with application to bearings and the washboard instability of a planing plate, J. Non-Newtonian Fluid Mech. (2012), doi:10.1016/j.jnnfm.2011.11.008

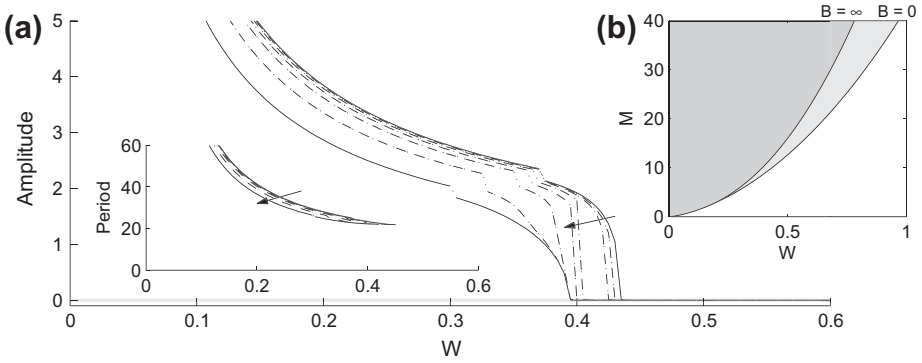

Fig. 16. (a) Amplitude and period of periodic oscillations of the plate for varying load $\mathcal{W}$, $\mathcal{M} = 10$, and for different values of the yield stress B. Solid lines show $B = 0$ and $B \to \infty$, whilst the dashed lines show $B = 0.01, 0.02, 0.05, 0.1, 0.2, 0.5$, with the arrow indicating the trend with increasing B. The dotted sections of the lines separate oscillations that are always in contact with the fluid from those that leave the surface. (b) Instability region of $\mathcal{W} - \mathcal{M}$ parameter space for the cases $B = 0$ (lighter shading) and $B = \infty$ (darker shading).

yield stress is sufficiently strong that the deformed fluid surface remains relatively steep near the edges of the splash pattern).

To illustrate this, we reintroduce gravity into the problem, taking its dimensionless size to be $\mathcal{G} = \rho g \mathcal{H}^2/\mathcal{TL}$, where g is the gravitational acceleration. The evolution of the free surface η is then given (for the Bingham fluid) by

$$\eta_t - \left[\eta + \frac{1}{6}\zeta^2(3\eta - \zeta)\mathcal{G}\eta_x\right]_x = 0, \quad \zeta = \left(\eta - \frac{B}{\mathcal{G}|\eta_x|}\right)_+, \tag{60}$$

with

$$\left[\eta + \frac{1}{6}\zeta^2(3\eta - \zeta)\mathcal{G}\eta_x\right]\Big|_{x=0} = -Q(t), \quad \eta_x \to 0 \text{ as } x \to -\infty, \tag{61}$$

where ζ is analogous to Y_- and represents the lower limit of a surface pseudo-plug [14,12,32,26].

To solve (60), we use finite differences on a uniform grid to evaluate the spatial derivatives, then integrate the resulting ordinary differential equations in time using a standard stiff integrator with a variable time step (MATLAB's ODE15s). However, special care is required in order to avoid unwanted numerical diffusion associated with the advection term, especially to compute the long-time evolution towards the final washboard pattern. We minimize such diffusion by actually solving (60) in the frame of the fluid layer. Having moved into that frame and defined the new spatial coordinate, $\xi = x + t$, the flux $-Q(t)$ is prescribed at the moving right-hand edge of the domain, $\xi = t$. To avoid spurious oscillations due to finite resolution, occurring as grid points move onto the computational grid in $\xi < t$, we replace the flux condition by a distributed source term, narrowly confined around $\xi = t$ (verifying that the width of the source does not affect the solution).

Fig. 17a shows a sample free surface pattern evolving from the forcing imposed by the periodic oscillation shown earlier in Fig. 15. Under gravity, the forcing pattern $-Q(x + t)$ collapses over the regions where $\eta|\eta_x| > B/\mathcal{G}$, invading the surrounding layers where fluid was initially deposited below the yield stress. The fluid subsequently brakes to rest once surface slopes become sufficiently shallow. As $t \to \infty$, the slumped regions are characterized by $\zeta \to 0$ (corresponding to an approach of the shear stress to the yield stress), indicating that the smoothed-out regions of the eventual pattern converge to profiles of the form,

$$\eta(\xi) \equiv \eta(x,t) = \sqrt{\eta_*^2 \pm \frac{2B}{\mathcal{G}}(x + t - \xi_*)}, \tag{62}$$

where ξ_* and $\eta_* = \eta(\xi_*)$ denote a given point and depth within the slumped region.

As shown in Fig. 17b, the spatial intervals occupied by the slumped sections of the profile depend on the gravitational param-

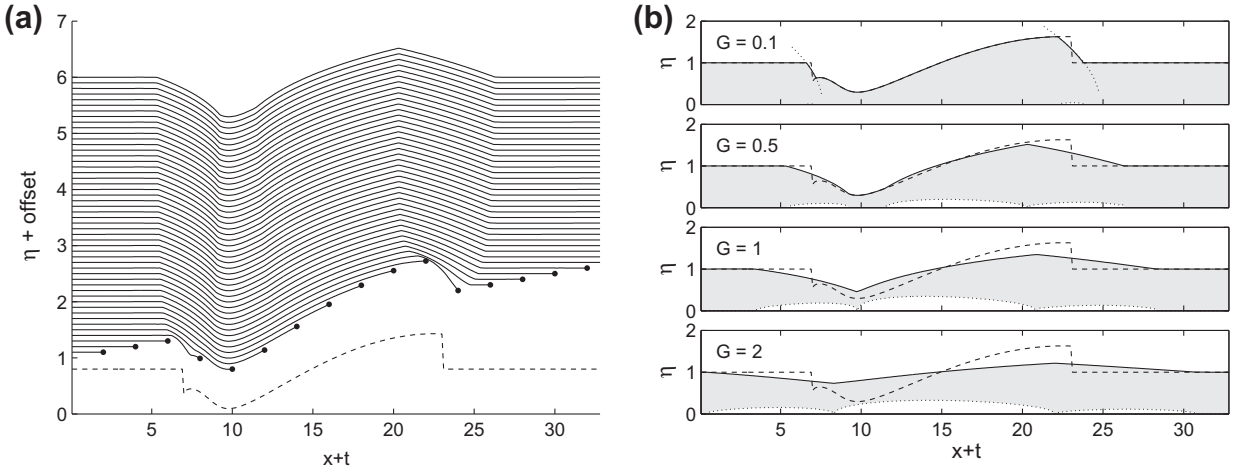

Fig. 17. (a) Free surface evolution governed by (60) and (61), resulting from the periodic oscillation of the plate in Fig. 15, with $\mathcal{M} = 10$, $B = 0.05$ and $\mathcal{G} = 0.5$. Solutions are shown every two time intervals between 0 and 100, offset vertically by $t/20$, with the dot showing the location of the plate tip ($x = 0$). The dashed line shows the shape of $-Q(x + t)$ for reference. Panel (b) shows similar solutions at $t = 100$ with the values of $\mathcal{G}$ indicated. The plugs and pseudo-plugs are shaded, and dashed lines show $-Q(x + t)$. Dotted lines in the top axes indicate the limiting slumped profiles in (62).

Please cite this article in press as: I.J. Hewitt, N.J. Balmforth, Viscoplastic lubrication theory with application to bearings and the washboard instability of a planing plate, J. Non-Newtonian Fluid Mech. (2012), doi:10.1016/j.jnnfm.2011.11.008

eter: if $\mathcal{G}$ is small, the profile remains largely unaltered from $-Q(x+t)$, but slumps over distinct, localized zones surrounding the discontinuities that arise from the entry and take-off of the paddle. For larger $\mathcal{G}$, further sections of the fluid layer collapse, and the slumps widen with time and merge together, smoothing out the final shape more significantly. Although the surface is now rendered continuous everywhere, the surface slope remains discontinuous at the edges of the slumped sections.

5. Discussion

In this paper, we have described a general method to compute stresses and flow fields in viscoplastic lubrication problems. The central difficulty in such problems is that the structure of the flow field, and the resulting relationships between pressure gradient and fluid velocity, are generally not known *a priori*, but must be determined as part of the solution. For example, the flow may contain fully yielded sections, genuine plugs attached to the walls, and floating pseudo-plugs, all of which come and go as the surfaces change position. The current formulation avoids any need to explicitly decompose the flow pattern into constituents of this kind and can be solved using an efficient numerical scheme.

We applied the theory to the viscoplastic journal bearing, deriving richer families of solutions than previously documented. Although typical bearing operating conditions may preclude any important impact of a yield stress (B is small in our dimensionless model), magneto-rheological fluids might present a novel application in which controlled yield stresses do play an elemental role, as remarked by Tichy [4]. Indeed, a recent article by Ewoldt et al. [33] illustrates how one can manipulate the yield stress over a thin fluid layer to control adhesion between the bounding solid surfaces.

In such applications it is important to understand the arrest of motion by the yield stress, motivating our analysis of the sedimentation of the inner cylinder within a journal bearing. In the bearing's thin geometry, lubrication theory can be exploited throughout the fluid, allowing a good deal of analytical headway into this problem. In more general geometries (such as sedimentation onto a planar surface), the lubrication approximation fails away from the thinnest sections of the intervening gap, which is where the yield stress arrests motion, precluding further analysis.

A main goal of this study was to examine the washboarding instability on a viscoplastic fluid layer. An earlier paper [16] presented a conceptual model of the problem, designed to complement experiments in which washboards were observed. That model was too crude to demonstrate definitively that washboard patterns emerge due to the linear instability of the steady planing state. Here, we have been able to shore up the idea with a model derived from the governing fluid equations, and, therefore, based more firmly on the detailed fluid mechanics. The theory may also be relevant to industrial processes such as blade coating: if the blade can deform in response to the fluid force (such designs are common, see [25]), the washboarding instability could be a concern.

The analysis suggests that to make the plate stable, one should increase the dimensionless weight or decrease the dimensionless inertia. On the other hand, the dimensional weight and inertia are likely related to one another, and it proves more helpful to think in terms of the velocity $\mathcal{U}$, with instability occurring above a critical speed, $\mathcal{U}_c$.[3] Washboarding is avoided if speeds are sufficiently slow, a solution which does not cut much mustard with drivers on roads. The model predictions, however, apply to a relatively shallow layer for which the fluid is forced to flow throughout its depth; when the layer is deeper, deformation is likely to be confined close to the surface and the stability conditions may be different.

A worthwhile extension of the analysis is to consider moving objects with different shapes. A parabolic shape is of interest for both washboarding with a wheel and for industrial roll-coating applications [23]. The formulation in Section 2 is not restricted to a flat plate, but the chief difficultly in extending the analysis lies in locating the separation point where the fluid detaches downstream. For the plate with its sharp edge, we can sensibly assume that the flow separates at the lowest point; but for more general shapes this is not the case. Additional separation conditions (see [34,35,23]) must be applied, and surface tension likely plays a more prominent role.

Finally, we have not considered the stability of our planing or washboarding solutions to perturbations in the third (lateral) dimension. Particularly when the vertical flow front at L is retreating, the flow may well become unstable to fingering, as in the printer's instability [36]. Indeed, in the experiments reported by Hewitt et al. [16] and illustrated in Fig. 1, the washboard patterns dug out by the oscillating plate often featured a serrated downstream edge, where the plate detached from the fluid; fingering just prior to detachment offers a plausible explanation.

Acknowledgement

IJH thanks the Killam Foundation for the support of a postdoctoral fellowship.

Appendix A. Newton iteration for lubrication flows

To solve (10), (14) and (16), assume that we have a trial solution for the surface stresses, $\check{\tau}_1$ and $\check{\tau}_2$, and the flux, $\check{Q}$. Then small corrections satisfy

$$F(\check{\tau}_1,\check{\tau}_2)+F_1\Delta\tau_1+F_2\Delta\tau_2\approx 0 \tag{A.1}$$

$$G(\check{\tau}_1,\check{\tau}_2,\check{Q})+G_1\Delta\tau_1+G_2\Delta\tau_2\approx \Delta Q \tag{A.2}$$

and

$$P-\int_D(\check{\tau}_2-\check{\tau}_1)\frac{\mathrm{d}x}{h}\approx\int_D(\Delta\tau_2-\Delta\tau_1)\frac{\mathrm{d}x}{h}, \tag{A.3}$$

where

$$F(\tau_1,\tau_2)=\frac{I_0(\tau_1)-I_0(\tau_2)}{\tau_1-\tau_2}-\frac{U}{h}, \tag{A.4}$$

$$G(\tau_1,\tau_2,\check{Q})=\frac{Uh(\tau_2+\tau_1)}{2(\tau_2-\tau_1)}-\frac{h^2[I_1(\tau_2)-I_1(\tau_1)]}{(\tau_2-\tau_1)^2}-\check{Q}+q, \tag{A.5}$$

$$F_j=\left.\frac{\partial F}{\partial\tau_j}\right|_{\tau_1=\check{\tau}_1,\tau_2=\check{\tau}_2}\quad\text{and}\quad G_j=\left.\frac{\partial G}{\partial\tau_j}\right|_{\tau_1=\check{\tau}_1,\tau_2=\check{\tau}_2}. \tag{A.6}$$

Thus, denoting $\check{F}=F(\check{\tau}_1,\check{\tau}_2)$ and $\check{G}=G(\check{\tau}_1,\check{\tau}_2,\check{Q})$,

$$\Delta\tau_j\approx\frac{(-1)^j}{J}[F_k\Delta Q-\check{G}F_k+\check{F}G_k], \tag{A.7}$$

where $J=F_1G_2-F_2G_1$ and $k=3-j$. Then,

$$\Delta Q\int_D(F_1+F_2)\frac{\mathrm{d}x}{hJ}\approx P-\int_D(\check{\tau}_2-\check{\tau}_1)\frac{\mathrm{d}x}{h}-\int_D[\check{F}(G_2+G_1)-\check{G}(F_1+F_2)]\frac{\mathrm{d}x}{hJ}. \tag{A.8}$$

In other words, after adopting a suitable discretization and quadrature rule with which to evaluate the various integrals, we may correct Q from (A.8), and then τ_j from (A.7). In practice, the first guess can be provided by the Newtonian solution, whereas later guesses can be taken from previous solutions or earlier time steps.

[3] If the plate's dimensional inertia is m, and weight mg, then our dimensionless inertia parameter, $\mathcal{M}=\mathcal{W}(\mathcal{H}/\mathcal{L})(\mathcal{U}^2/g\mathcal{L})$. But Fig. 16b indicates that $\mathcal{M}$ must typically be rather larger than $\mathcal{W}$ for instability to occur. Thus, $\mathcal{U}$ should be large relative to $g\mathcal{L}=g\mathcal{H}/\tan\alpha$ to destabilize steady planing.

Please cite this article in press as: I.J. Hewitt, N.J. Balmforth, Viscoplastic lubrication theory with application to bearings and the washboard instability of a planing plate, J. Non-Newtonian Fluid Mech. (2012), doi:10.1016/j.jnnfm.2011.11.008

Note that the iteration involves purely vector operations, and is therefore relatively fast.

Appendix B. Flow configurations

For the Herschel–Bulkley model

$$\Gamma(\tau) = \mathrm{sgn}(\tau)(|\tau| - B)_+^{1/n}, \tag{B.1}$$

$$I_0(\tau) = \frac{n}{n+1}(|\tau| - B)_+^{1+1/n}, \tag{B.2}$$

$$I_1(\tau) = \mathrm{sgn}(\tau)\left[B + \frac{n+1}{2n+1}(|\tau| - B)_+\right] I_0(\tau), \tag{B.3}$$

where $(\cdot)_+$ indicates $\max(\cdot, 0)$. If

$$\sigma_j = |\tau_j| - B \quad \text{and} \quad s_j = \mathrm{sgn}(\tau_j), \tag{B.4}$$

then the stress relationships (10) and (14) are rewritten as

$$\frac{U}{h} = \frac{n(\sigma_{2+}^{1+1/n} - \sigma_{1+}^{1+1/n})}{(n+1)[(s_2 - s_1)B + s_2\sigma_2 - s_1\sigma_1]}, \tag{B.5}$$

$$\frac{2(n+1)}{nh^2}(Q-q) = \frac{n\left(s_2\sigma_{2+}^{2+1/n} - s_1\sigma_{1+}^{2+1/n}\right)}{(2n+1)[(s_2 - s_1)B + s_2\sigma_2 - s_1\sigma_1]^2} - \frac{\left(\sigma_{2+}^{1+1/n} + \sigma_{1+}^{1+1/n}\right)}{[(s_2 - s_1)B + s_2\sigma_2 - s_1\sigma_1]}. \tag{B.6}$$

B.1. Central pseudo-plug (region A); $|\tau_1|$, $|\tau_2| > B$, $s_1 = -s_2$

In this case there are no further simplifications of the full algebraic expressions in (B.5) and (B.6), except in the limit of large B or low surface speeds. In those cases, $\sigma_j \ll B$ and a number of terms disappear from the leading-order balances, to furnish

$$\begin{pmatrix}\sigma_1\\ \sigma_2\end{pmatrix} \sim \left[\frac{2Bs_1}{nh^2}(n+1)\left(Q - q \pm \frac{1}{2}hU\right)\right]^{n/(n+1)}. \tag{B.7}$$

Also,

$$p_x \sim \frac{2s_2 B}{h}. \tag{B.8}$$

The positions of the yield surfaces are given to leading order by

$$Y_- \sim Y_1 + \frac{h}{2B}\sigma_1, \quad Y_+ \sim Y_2 - \frac{h}{2B}\sigma_2, \tag{B.9}$$

and are therefore $O(U^{n/(n+1)}B^{-1/(n+1)})$ from the walls (see Fig. 5).

B.2. Lower plug (region B); $|\tau_2| \geqslant B$, $|\tau_1| < B$

With $|\tau_1| < B$, $\sigma_{1+} = 0$ and (B.5) and (B.6) then determine σ_2 to be

$$\sigma_2 = \left[\frac{(n+1)s_2U^2}{(2n+1)(Q - q + \frac{1}{2}hU)}\right]^n. \tag{B.10}$$

Hence

$$\tau_1 = Bs_2 + s_2\sigma_2\frac{(2n+1)(Q-q) + \frac{1}{2}hU}{(2n+1)(Q - q + \frac{1}{2}hU)}, \tag{B.11}$$

$$p_x = \frac{ns_2\sigma_2 U}{(2n+1)(Q - q + \frac{1}{2}hU)}. \tag{B.12}$$

The yield surface at the top of the plug is given by

$$Y_+ = Y_2 - \frac{2n+1}{n}\frac{Q - q + \frac{1}{2}hU}{U}. \tag{B.13}$$

The borders of this region occur for $\tau_1 \to \pm Bs_2$, corresponding to connections to a C or an A region, respectively. In the limit of large B or low surface speed (when Q and q are both order $U \ll 1$), we observe from (B.10) that σ_2 is $O(U^n)$ throughout most of the B region. However, over a slender zone with a thickness of order $U^{n/(n+1)}B^{-1/(n+1)}$ adjoining the transition point to region A, this extra stress diverges to become $O(U^{n/(n+1)}B^{n/(n+1)})$, allowing τ_1 to approach $-B\,s_2$ in (B.11).

B.3. Upper plug (region D); $|\tau_1| \geqslant B$, $|\tau_2| < B$

Similarly, with $|\tau_2| < B$, $\sigma_{2+} = 0$ and we find

$$\sigma_1 = \left[-\frac{(n+1)s_1U^2}{(2n+1)(Q - q - \frac{1}{2}hU)}\right]^n, \tag{B.14}$$

and hence

$$\tau_2 = Bs_1 + s_1\sigma_1\frac{(2n+1)(Q-q) - \frac{1}{2}hU}{(2n+1)(Q - q - \frac{1}{2}hU)}, \tag{B.15}$$

$$p_x = \frac{ns_1\sigma_1 U}{(2n+1)(Q - q - \frac{1}{2}hU)}. \tag{B.16}$$

The yield surface at the bottom of the plug is given by

$$Y_- = Y_1 - \frac{2n+1}{n}\frac{Q - q - \frac{1}{2}hU}{U}. \tag{B.17}$$

The D region is bordered by the points where $\tau_1 = \pm Bs_1$, corresponding to transitions to C and A regions. Once again, $\sigma_1 = O(U^n) \ll B$ in the large yield stress or low surface speed limit, except within a slender zone adjacent to the transition to A, where σ_1 becomes $O(U^{n/(n+1)}B^{n/(n+1)})$.

B.4. Fully yielded (region C); $|\tau_1|$, $|\tau_2| > B$, $s_1 = s_2$

In this case B drops out from the stress relationships (B.5) and (B.6), but for general n, no further progress can be made. For $n = 1$, the equations are identical to those for the Newtonian case, and have the solution

$$s_1\sigma_1 = \frac{U}{h} + \frac{6}{h^2}(Q-q), \quad s_2\sigma_2 = \frac{U}{h} - \frac{6}{h^2}(Q-q), \tag{B.18}$$

$$p_x = -\frac{12}{h^3}(Q-q), \tag{B.19}$$

(which indicate that $s_1 = s_2$ must have the sign of U).

B.5. Boundaries between regions

Given the explicit formulae for regions B and D, we may determine the borders between the four configurations:

$$x_{AB}: 2B + \frac{(2n+1)(Q-q) + \frac{1}{2}hU}{(2n+1)(Q - q + \frac{1}{2}hU)}\sigma_2 = 0, \tag{B.20}$$

$$x_{BC}: Q - q + \frac{1}{2(2n+1)}hU = 0, \tag{B.21}$$

$$x_{CD}: Q - q - \frac{1}{2(2n+1)}hU = 0, \tag{B.22}$$

$$x_{AD}: 2B + \frac{(2n+1)(Q-q) - \frac{1}{2}hU}{(2n+1)(Q - q - \frac{1}{2}hU)}\sigma_1 = 0. \tag{B.23}$$

In the limit of large B or low surface speed, $\sigma_j \ll B$, and so the first and last of these formulae reduce to

$$\begin{aligned} x_{AB}: &\quad Q \sim q - \frac{1}{2}Uh,\\ x_{AD}: &\quad Q \sim q + \frac{1}{2}Uh. \end{aligned} \tag{B.24}$$

Please cite this article in press as: I.J. Hewitt, N.J. Balmforth, Viscoplastic lubrication theory with application to bearings and the washboard instability of a planing plate, J. Non-Newtonian Fluid Mech. (2012), doi:10.1016/j.jnnfm.2011.11.008

B.5.1. Steady states

In the steady states of our example problems (*ie.* when $\dot{\varepsilon}, \dot{\Theta}$ or $\dot{Y}$ are zero), the commonly appearing terms $Q - q \pm \frac{1}{2}hU$ are $Q - hU_1$ and $Q - hU_2$. Since either the upper or lower surface is always at rest, one of these terms is simply Q and is therefore independent of x. In that case, one or other of regions B and D has constant pressure gradient and a yield surface that is independent of x (see Fig. 7(h) and Fig. 11).

Appendix C. The lift force on the rigid plate without pseudo-plugs

For the washboarding problem with the Bingham fluid, we have $q = \dot{Y}x - \frac{1}{2}h$ and $h = Y + x$. The boundaries between regions B, C and D in that case are given by

$$x_{BC} = -\frac{3Q + 2Y}{2 - 3\dot{Y}}, \quad x_{CD} = -\frac{3Q + Y}{1 - 3\dot{Y}}. \tag{C.1}$$

The boundaries with region A, x_{AB} and x_{AD}, are given respectively by the roots of the quadratic Eqs. (B.20) and (B.23). For large B, these positions tend to the limits

$$x_{AB} \sim -\frac{Q + Y}{1 - \dot{Y}}, \qquad x_{AD} \sim \frac{Q}{\dot{Y}}, \tag{C.2}$$

If x_{AB} and x_{AD} lie outside $0 < x < L$, there is no region A, and the analytical expressions for the pressure gradient in (B.12), (B.16) and (B.19) can be integrated to determine the flux:

$$Q = -\frac{Y[(Y + L) - \dot{Y}L]}{2Y + L}. \tag{C.3}$$

Having calculated Q, it may then be verified whether the boundaries of region A are indeed outside of $0 < x < L$. When the plate is not moving vertically, $\dot{Y} = 0$, and the condition for there to be no region A (the most restrictive condition is $x_{AB} < 0$) becomes (51); if L is further prescribed by (57), we arrive at (58).

If the calculated flux confirms that there is no A region, the force can be calculated by integrating the known pressure distribution. The result depends upon how the remaining B, C, or D regions are organized within the flow pattern. It turns out the only feasible arrangements are B-C-D, D–C–B, and the fully yielded case C. For the arrangement B-C-D (which can be shown to occur when $3L\dot{Y} < L - Y$), we find

$$\begin{aligned} f = {} & \frac{2(3L\dot{Y} - L + Y)}{9\dot{Y}(1 - \dot{Y})(Y + L\dot{Y})} - 6(1 - 2\dot{Y}) \log\left(\frac{1 - 3\dot{Y}}{2 - 3\dot{Y}}\right) \\ & - 4 + \frac{2}{9\dot{Y}^2} \log\left[\frac{(1 - 3\dot{Y})(Y + L\dot{Y})}{Y(1 - 2\dot{Y})}\right] \\ & + \frac{2}{9(1 - \dot{Y})^2} \log\left[\frac{(2 - 3\dot{Y})(Y + L\dot{Y})}{(1 - 2\dot{Y})(Y + L)}\right]; \end{aligned} \tag{C.4}$$

for C alone (occurring when $L - Y \leqslant 3L\dot{Y} \leqslant 2L + Y$),

$$f = 12(1 - 2\dot{Y})\left[\frac{1}{2}\log\left(\frac{Y + L}{Y}\right) - \frac{L}{2Y + L}\right]; \tag{C.5}$$

and for D-C-B (which arises for $3L\dot{Y} > 2L + Y$),

$$\begin{aligned} f = {} & \frac{2(3L\dot{Y} - 2L - Y)}{9\dot{Y}(1 - \dot{Y})(Y + L - L\dot{Y})} + 6(1 - 2\dot{Y}) \log\left(\frac{1 - 3\dot{Y}}{2 - 3\dot{Y}}\right) \\ & + 4 - \frac{2}{9\dot{Y}^2} \log\left[\frac{(1 - 3\dot{Y})(Y + L - L\dot{Y})}{(1 - 2\dot{Y})(Y + L)}\right] \\ & - \frac{2}{9(1 - \dot{Y})^2} \log\left[\frac{(2 - 3\dot{Y})(Y + L - L\dot{Y})}{Y(1 - 2\dot{Y})}\right]. \end{aligned} \tag{C.6}$$

In the steady state, when $\dot{Y} = 0$, the expressions in (C.4)–(C.6) reduce to (50). The horizontal force on the plate can similarly be calculated in these cases, integrating the expressions for the stress in (B.11), (B.14) and (B.18).

Appendix D. Free surfaces adjacent to the washboarding plate

The planing solution in Section 4 includes jumps in surface height at the leading and trailing edges, which in reality are smoothed out by some combination of surface tension, gravity, and fully two-dimensional flow. With gravity alone, the free surface height η satisfies (60). Upstream of the plate, the appropriate boundary conditions are

$$\eta(L, t) = h(L, t) \equiv Y(t) + L(t), \quad \eta \to 1 \text{ as } x \to \infty. \tag{D.1}$$

The flux at $x = L$ is then $-\left[\eta + \frac{1}{6}\zeta^2(3\eta - \zeta)\mathcal{G}\eta_x\right]_{x=L}$. In the washboarding model of Section 4, this flux is taken equal to the upstream value -1, and then used to determine the motion of the leading edge *via* the jump condition (53). In principle, however, the flux is determined from solving (60) subject to (D.1), then matching the solution to that for the flow underneath the plate at $x = L(t)$, leading to a coupled system of equations describing both regions.

Nevertheless, if $B/\mathcal{G} \gg 1$, the free-surface region over which gravity has an effect is small and we may rescale near the leading edge, $x = L + X\mathcal{G}/B$, so that the time derivative in (60) drops out to leading order. The flux is then approximately given by -1, and so

$$\eta + \frac{1}{6}\zeta^2(3\eta - \zeta)B\eta_X = 1, \quad \zeta = (\eta - 1/|\eta_X|)_+. \tag{D.2}$$

This relation must be solved to match to the depth, $Y(t) + L(t)$, of the plate at $X = 0$; some example solutions are shown in Fig. D.18. If B is large, a pseudo-plug occupies the bulk of the layer ($\zeta \sim B^{-1/2}$) and the upstream surface profile is given by

$$\eta(x, t) \sim \begin{cases} \sqrt{(Y + L)^2 - 2(x - L)B/\mathcal{G}}, \\ 1, \end{cases} \tag{D.3}$$

for $(x - L) < \frac{1}{2}[(Y + L)^2 - 1]\mathcal{G}/B$ and $(x - L) \geqslant \frac{1}{2}[(Y + L)^2 - 1]\mathcal{G}/B$ respectively, as shown in Fig. D.18c.

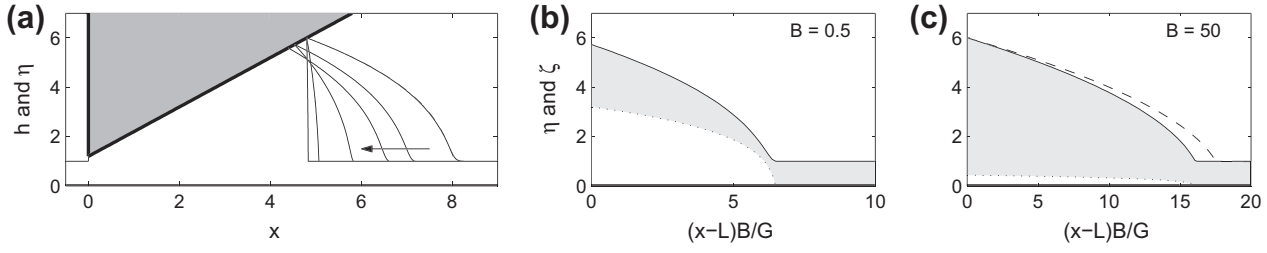

Fig. D.18. (a) Steady state free surface shapes at leading edge according to (D.1) and (D.2), for the steady planing plate with $Y = 1.2$, $\mathcal{G} = 0.1$, and for $B = 0, 0.05, 0.1, 0.5, 5, 50$ (the arrow indicates the trend with increasing B). Note the value of L, where the free surface meets the plate, varies with B as in Fig. 12. Panels (b) and (c) show close-ups of the transition region for the cases $B = 0.5$ and $B = 50$, with the shading denoting the pseudo-plug. The dashed line in (c) shows the square-root solution in (D.3).

Please cite this article in press as: I.J. Hewitt, N.J. Balmforth, Viscoplastic lubrication theory with application to bearings and the washboard instability of a planing plate, J. Non-Newtonian Fluid Mech. (2012), doi:10.1016/j.jnnfm.2011.11.008

It turns out that gravity is not sufficient to enforce continuity at the trailing edge of the plate; instead we must include surface tension or solve the full two-dimensional Stokes problem. Discussion of related Newtonian problems is given by Tuck & Schwartz [37], Moriarty and Terrill [38] and Quintans Carou et al. [39].

References

[1] O. Pinkus, B. Sternlicht, Theory of Hydrodynamic Lubrication, McGraw-Hill, New York, 1961.
[2] D. Dowson, Elastohydrodynamic and Micro-elastohydrodynamic lubrication, Wear 190 (1995) 125–138.
[3] A.A. Milne, A theory of rheodynamic lubrication, Colloid Polym. Sci. 139 (1954) 96–101.
[4] J.A. Tichy, Hydrodynamic lubrication theory for the Bingham plastic flow model, J. Rheol. 35 (1991) 477–506.
[5] M. Moyers-Gonzalez, I.A. Frigaard, C. Nouar, Stable two-layer flows at all Re; visco-plastic lubrication of shear-thinning and viscoelastic fluids, J. non-Newt. Fluid Mech. 165 (2010) 1578–1587.
[6] K. Vajravelu, S. Sreenadh, V. Ramesh Babu, Peristaltic transport of a Herschel–Bulkley fluid in an inclined tube, Int. J. Nonlinear Mech. 40 (1) (2005) 83–90.
[7] D. Takagi, Nonlinear peristaltic waves, in: Proceedings of the Geophysical Fluid Dynamics Summer Study Program, Woods Hole Oceanopgraphic Institution, WHOI-2010-01, 2010.
[8] N.J. Balmforth, D. Coombs, S. Pachman, Microelastohydrodynamics of swimming organisms near solid boundaries in complex fluids, Quart. J. Mech. Appl. Math. 63 (2010) 267–294.
[9] M.W. Denny, The role of gastropod mucus in locomotion, Nature 285 (1980) 160–161.
[10] D. Chan, N.J. Balmforth, A. Hosoi, Building a better snail: lubrication theory and adhesive locomotion, Phys. Fluids 17 (2005) 113101.
[11] I.C. Walton, S.H. Bittleston, The axial flow of a Bingham plastic in a narrow eccentric annulus, J. Fluid Mech. 222 (1991) 39–60.
[12] N.J. Balmforth, R.V. Craster, A consistent thin-layer theory for Bingham fluids, J. Non-Newt. Fluid Mech. 84 (1999) 65–81.
[13] R.L. Batra, Rheodynamic lubrication of a journal bearing, Appl. Sci. Res. A 15 (1966) 331–344.
[14] K.F. Liu, C.C. Mei, Slow spreading of Bingham fluid on an inclined plane, J. Fluid Mech. 207 (1989) 505–529.
[15] S. Pegler, Snail locomotion, in: Proceedings of the Geophysical Fluid Dynamics Summer Study Program, Woods Hole Oceanopgraphic Institution, WHOI-2011-01, 2010.
[16] I.J. Hewitt, N.J. Balmforth, J.N. McElwaine, Granular and fluid washboards. J. Fluid Mech. (in press)
[17] A. Beris, J. Tsamopoulos, R.A. Brown, R.C. Armstrong, Creeping motion of a sphere through a Bingham plastic, J. Fluid Mech. 158 (1985) 219–244.
[18] A. Putz, I.A. Frigaard, Creeping flow around particles in a Bingham fluid, J. Non-Newt. Fluid Mech. 165 (2010) 263–280.
[19] H. Brenner, The slow motion of a sphere through a viscous fluid towards a plane surface, Chem. Eng. Sci. 16 (1961) 242.
[20] K.B. Mather, Why do roads corrugate?, Scientific American 208 (1963) 128–136
[21] N. Taberlet, S.W. Morris, J.N. McElwaine, Washboard road: the dynamics of granular ripples formed by rolling wheels, Phys. Rev. Lett. (2007) 99.
[22] A. Bitbol, N. Taberlet, S.W. Morris, J.N. McElwaine, Scaling and dynamics of washboard roads, Phys. Rev. E 79 (2009) 79.061308.
[23] K.J. Ruschak, Coating flows, Ann. Rev. Fluid Mech. 17 (1985) 65–89.
[24] T.P. Witelski, Dynamics of air bearing sliders, Phys. Fluids 10 (1998) 698–708.
[25] F.A. Saita, Simplified models of flexible blade coating, Chem. Eng. Sci. 44 (1989) 817–825.
[26] N.J. Balmforth, R.V. Craster, A.C. Rust, R. Sassi, Viscoplastic flow over an inclined surface, J. Non-Newt. Fluid Mech. 139 (2006) 103–127.
[27] S. Wada, H. Hayashi, K. Haga, Behavior of a Bingham solid in hydrodynamic lubrication (Part 1. General theory), Bull. Jpn. Soc. Mech. Eng. 16 (1973) 422–431.
[28] G.P. Matson, A.J. Hogg, Two-dimensional dambreak flows of Herschel–Bulkley fluids: the approach to the arrested state, J. Non-Newton. Fluid Mech. 142 (2007) 79–94.
[29] R. Huilgol, B. Mena, J.M. Piau, Finite stopping time problems and rheometry of Bingham fluids, J. Non-Newton. Fluid Mech. 102 (2002) 97–107.
[30] C. Dorier, J. Tichy, Behaviour of a Bingham-like viscous fluid in lubrication flows, J. Non-Newton. Fluid Mech. 45 (1992) 291–310.
[31] Y. Greener, S. Middleman, Blade-coating of a viscoelastic fluid, Polym. Eng. Sci. 14 (1974) 791–796.
[32] A.B. Ross, S.K. Wilson, B.R. Duffy, Thin-film flow of a viscoplastic material round a large horizontal stationary or rotating cylinder, J. Fluid Mech. 430 (2001) 309–333.
[33] R.H. Ewoldt, P. Tourkine, G.H. McKinley, A.E. Hosoi, Controllable adhesion using field-activated fluids, Phys. Fluids 23 (2011) 073104.
[34] G.I. Taylor, Cavitation of a viscous fluid in narrow passages, J. Fluid Mech. 16 (1963) 595–619.
[35] M.D. Savage, Mathematical models for coating processes, J. Fluid Mech. 117 (1982) 443–455.
[36] J.R.A. Pearson, The stability of uniform viscous flow under rollers and spreaders, J. Fluid Mech. 7 (1960) 481–500.
[37] E.O. Tuck, L.W. Schwartz, A numerical and asymptotic study of some third-order ordinary differential equations relevant to draining and coating flows, SIAM Rev. 32 (1990) 453–469.
[38] J.A. Moriarty, E.L. Terrill, Mathematical modelling of the motion of hard contact lenses, Euro. J. Appl. Math. 7 (1996) 575–594.
[39] J. Quintans Carou, S.K. Wilson, N.J. Mottram, B.R. Duffy, Asymptotic and numerical analysis of a simple model for blade coating, J. Eng. Math. 63 (2009) 155–176.

Please cite this article in press as: I.J. Hewitt, N.J. Balmforth, Viscoplastic lubrication theory with application to bearings and the washboard instability of a planing plate, J. Non-Newtonian Fluid Mech. (2012), doi:10.1016/j.jnnfm.2011.11.008